(a) Model 1

(b) Model 2

Figure 2. Two models of P450s used in this study.

(a) Fe-S bond bending (b) Fe-S-C angle bending (c) Torsional rotation around Fe-S

(d) Du1-Fe stretching

Du1: dummy atom located in the center of four nitrogens

(e) Du2-Fe-S bending

Du2: dummy atom located in the place where Du1-Fe-Du2 = 90°

Figure 3. Structural changes to calculate energy profiles for the parameterization of P450s.

combination of quantum chemical methods and basis sets used for each model.

The atomic charges necessary for MM and CMD methods were calculated from the optimized structure. To apply these charges in calculations using whole P450s, atomic charges were computed for the more complex model 1 using method III. Various techniques for atomic charge calculations using quantum chemical methods have been proposed.[27–31] This study used RESP method,[30,31] which is a modified version of Merz-Kollman method[29] that is known to generate suitable charges for MM and CMD. RESP charge is obtained to reproduce the electrostatic potential and is recommended for AMBER,[32] which is one of the most widely used CMD programs. In AMBER program, total charges of amino acid residues are defined as integer values when the ACE and
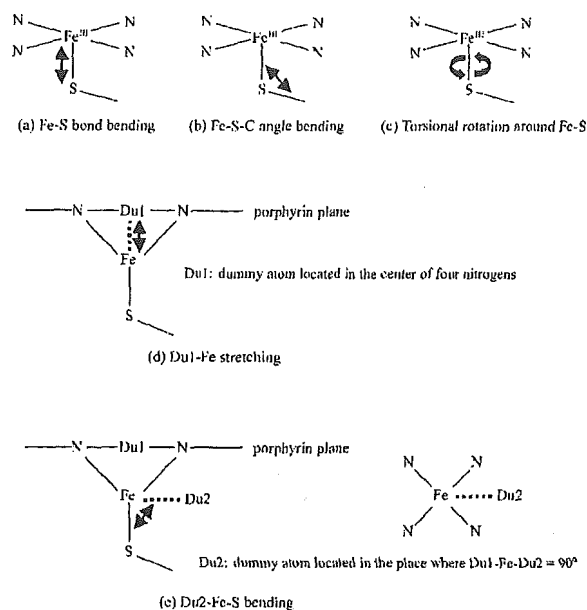
NME groups are removed.[31] Therefore, the total charge of model 1 was defined as −2 when the ACE and NME were removed. The previously defined values of atomic charges for ACE and NME were used.[31]

Model 2 was used to calculate the force field parameters. As shown in Figure 3, energy changes with Fe—S bond bending, Fe–S–C angle bending and torsional motion around Fe—S were calculated using quantum chemical methods, and parameter fitting was carried out using calculated energy profiles. In addition to

Table 1. Quantum Chemical Methods Used in This Study.

(a) Model 1		
	I	III
Method	AM1	UHF
Basis sets for H, C, N, O and S	AM1	3-21G*
Basis sets for Fe(III)	AM1	MIDI[a]

(b) Model 2								
	i	ii	iii	iv	v	vi	vii	viii	ix
Method	AM1	UHF	UHF	UHF	UHF	UHF	UHF	UB3LYP	UB3LYP
Basis sets for H, C, N and S	AM1	3-21G*	3-21G*	4-31G*	4-31G*	6-31G*	6-31G*	4-31G*	4-31G*
Basis sets for Fe(III)	AM1	3-21G*	MIDI[a]	6-31G*	MIDI[a]	6-31G*	MIDI[a]	6-31G*	MIDI[a]

[a]Tatewaki-Huzinaga MIDI plus Hay's diffuse basis sets.

parameters around Fe—S, parameters for interactions between iron and porphyrin were also determined to reproduce the location of the iron atom, which is out of porphyrin plane in high-spin state. To caclulate these parameters, only Fe—SCH₃ moiety was moved along Du1–Fe (Du1 was a dummy atom located in the center of four nitrogen atoms) and Du2–Fe–C (Du2 was a dummy atom located in the place where angle Du1–Fe–Du2 is equal to 90°) as shown in Figure 3d and c, respectively, and the energy profiles were calculated. For this purpose, the least-square method was performed to minimize the standard deviation (SD) in eq. (1),

$$SD = \sum (E(QC) - E(MM))^2 \qquad (1)$$

where $E(QC)$ is the energy calculated through quantum chemical methods and $E(MM)$ is obtained using the force field. These calculations used UB3LYP with the MIDI basis sets for iron and 4-31G* for other elements. PARM94 parameters[33] [eq. (2)] in AMBER were adopted as the force field,

$$E_{total} = \sum_{bonds} K_r(r - r_{eq})^2 + \sum_{angles} K_\theta(\theta - \theta_{eq})^2$$

$$+ \sum_{dihedrals} \frac{V_n}{2}[1 + \cos(n\phi - \gamma)] + \sum_{i<j}\left(\frac{A_{ij}}{R_{ij}^{12}} - \frac{B_{ij}}{R_{ij}^6} + \frac{q_iq_j}{\varepsilon R_{ij}}\right) \qquad (2)$$

where the first and second terms, which are related to bond stretching and angle bending, respectively, express the harmonic-oscillator approximations. The parameters r_{eq} and θ_{eq} are equilibrium bond length and bond angle, and K_r and K_θ are force constants. The third term is the torsional term, where V_n is the energy barrier of torsional motion, n is the periodicity and γ is the phase. The last term describes nonbonded interactions. In this study, AMBER PARM94 and Giammona's parameters (http://pharmacy. man.ac.uk/amber/) were used to calculate the energies of iron-porphyrin systems, with the exception of parameters around iron atom.

To validate the parameters obtained, MM calculations of P450cam with five-coordinated Fe(III) were carried out and the structures were compared before and after the calculations. The experimental crystal structure determined by X-ray diffraction (PDB ID: 2CPP)[34] was used for the initial structure of P450cam. Because hydrogen atoms were not determined in this experimental structure, they were added by using the "Protonate" module of AMBER 6.[32] Furthermore, the side-chain atoms of Lys214, which were missing in the crystal structure, were added using the "Biopolymer" module of SYBYL6.9.2.[35] In the first step of the MM calculation on P450cam, only the added hydrogens and side-chain atoms were optimized. An MM optimization of all atoms in P450cam was then carried out. For all MM calculations, the first 1000 steps were completed using the steepest-descent method, and the rest of the calculation was carried out using the conjugate-gradient method until the energy gradient became less than 0.01 kcal/mol Å. A cutoff distance of 18.0 Å for nonbonded interactions and a constant dielectric coefficient of $\varepsilon = 77.9$ were used in the refinement.

AM1 calculations were carried out using MOPAC2002.[36] UHF and UB3LYP calculations were performed using Gaussian98.[37]
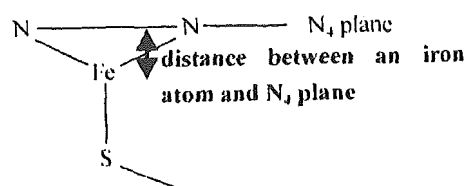

Figure 4. Distance between iron atom and N₄ plane.

The calculation of RESP charges and the MM calculations on P450cam, carried out to validate the force field parameters around Fe—S, were completed using AMBER 6.[32] An SGI OCTANE workstation with MIPS R12000 dual processors and IRIX 6.5 were used.

Results and Discussions

After optimization using the same methods, the structures of models 1 and 2 were compared. Some of the bond lengths, bond angles, and distances between the iron atom and N₄ plane (illustrated in Fig. 4) are shown in Table 2 (Other bond length and bond angles are illustrated in Supplementary Material). In addition to the computational results, experimentally determined structures for high-spin state P450, homologous enzyme, and model compounds with five-coordinated Fe(III) are also described. Four experimental results are mentioned: EXAFS 1, which is the structure of P450cam using extended X-ray-absorption fine structure (EX-AFS);[38] EXAFS 2, which is the structure of chloroperoxidase from EXAFS;[39] X-ray 1, which is the structure of P450cam by X-ray diffraction;[34] and X-ray 2, which is the structure of Fe(PPIXDME)(SC₆H₄NO₂) by X-ray crystallography.[40] Computationally determined bond lengths are compared in Figure 5. As the tables and the figures show, all of the structural features were similar between model 1 and 2, with the exception of bond lengths and angles related to the iron atom obtained by AM1. Using UHF methods, the differences in bond length between the two models were within 10⁻² Å, with the exception of Fe—S bond length, and the differences in bond angles were all within 1°. The structural differences calculated by AM1 methods without structural features near the iron atom were similar to the UHF results. These results suggest that the more simplified model 2 is sufficiently accurate to calculate the structural features of iron-porphyrin systems. Because the numbers of atoms in models 1 and 2 were 95 and 42, respectively, the use of the latter for quantum calculations would reduce computational time and costs. The results of the superposition of the two models are illustrated in Figure 6. The root-mean-square deviations (RMSDs) of the porphyrin moieties between the two models were calculated as 0.142 Å and 0.068 Å using the AM1 and UHF methods, respectively. If experimental structure determination is repeated on the same protein, experimental error and the dynamic nature of proteins leads to RMSDs of approximately 0.4 Å.[41] In comparison, the RMSDs from these computationally optimized structures are small. These results also indicate that model 2 would be suitable for investigations into the structural features of P450s.

Table 2. Optimized Structures of Model 1 and 2.

	(a) Bond lengths around Fe/Å							
Method	EXAFS 1	EXAFS 2	X-ray 1	X-ray 2	I	i	III	iii
Fe—S	2.23	2.30	2.20	2.324	2.209	2.242	2.532	2.482
Fe—N	2.06	2.05	2.05	2.064	2.114	2.038	2.170	2.163

	(b) Bond angles around Fe/degree					
Method	X-ray 1	X-ray 2	I	i	III	iii
N_α—Fe—N_α	155.6	155.7	152.7	167.0	145.2	144.7
N_α—Fe—N_β	87.4	87.5	86.8	89.3	84.9	84.7

	(c) Distances between N_4 plane and Fe/Å					
Method	X-ray 1	X-ray 2	I	i	III	iii
N_4—Fe	0.43	0.434	0.498	0.231	0.648	0.655

The structures of model 1 and 2 optimized by AM1 and UHF are compared with experimental structures.

Following on from the results mentioned previously, geometry optimizations of model 2 were carried out using more accurate methods. The results are shown in Table 3, in which some of bond lengths, bond angles, and distances between the N_4 plane and the iron atom are described in the same way as in Table 2 (other structural features were shown in Supplementary Material). For structural features not related to the iron atom, almost all of the computational results reproduced the experimental results, with only a few exceptions when using methods ii and iii. However, for structural features around the iron atom, none of the UHF methods gave reasonable results compared with the experimental data. These results indicate that the UHF method is inadequate for

quantum chemical elucidation of P450 structures. Although method vii required a much longer time to complete the calculation than method v, the structural features calculated using methods v and vii were similar. In fact, method v occasionally gave better results than method vii (e.g., the results for the bond length of C_α-C_β). Fast and accurate calculations are desirable for the preparation of MM and CMD, because many calculations are required to obtain energy profiles. Therefore, the 4-31G* basis set seems to be more suitable for H, C, N, and S atoms than 6-31G*.

The AM1 method produced reasonable values for Fe—S and Fe—N bond lengths, which indicates that AM1-d parameters are effective in calculating bond lengths. However, despite this find-
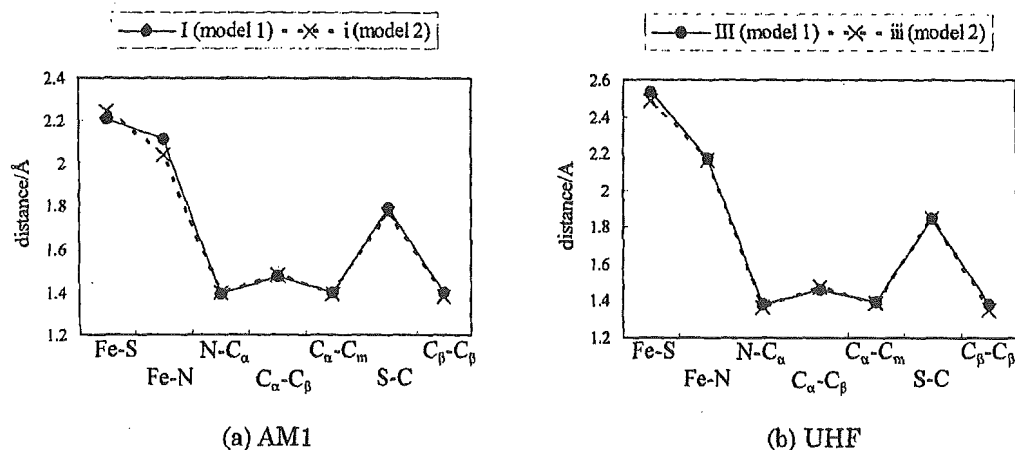

(a) AM1   (b) UHF

Figure 5. Comparisons of bond lengths in model 1 and 2 optimized by quantum chemical calculations.
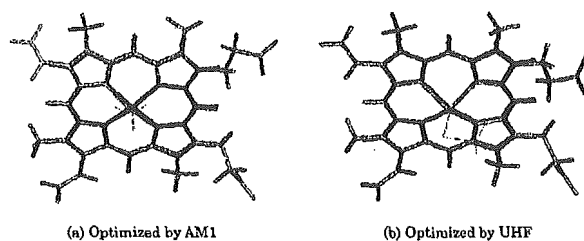
(a) Optimized by AM1   (b) Optimized by UHF

Figure 6. Superposition of model 1 and 2. Model 1 is illustrated in light gray and model 2 in dark gray.

ing, the AM1 method was inadequate for the accurate modeling of P450s, because the N–Fe–N angles and the distance between the N_4 plane and the iron differed from the experimental values. On the other hand, AM1 is a semiempirical method and is therefore not very time-consuming. For example, the computation time for optimizing model 2 was only a few minutes. The results of AM1 calculations were more accurate than those of *ab initio* UHF methods. Therefore, AM1 could to be appropriate for rough approximations or the initial calculations of more accurate methods.

The UB3LYP method viii, in which the 6-31G* basis set was used for iron, produced the same results as UHF. However, the results from method ix, in which the MIDI basis set was used for iron, were in good agreement with experimental structures around the heme iron. In particular, reasonable values for the distance between the N_4 plane and the iron atom, the N_α–Fe–N_α angle and the N_α–Fe–N_β angle, were obtained only with method ix. These results indicate that a UB3LYP method with the MIDI basis set for iron and 4-31G* for the other elements is the most suited to calculations of P450s. In addition, when comparing methods viii
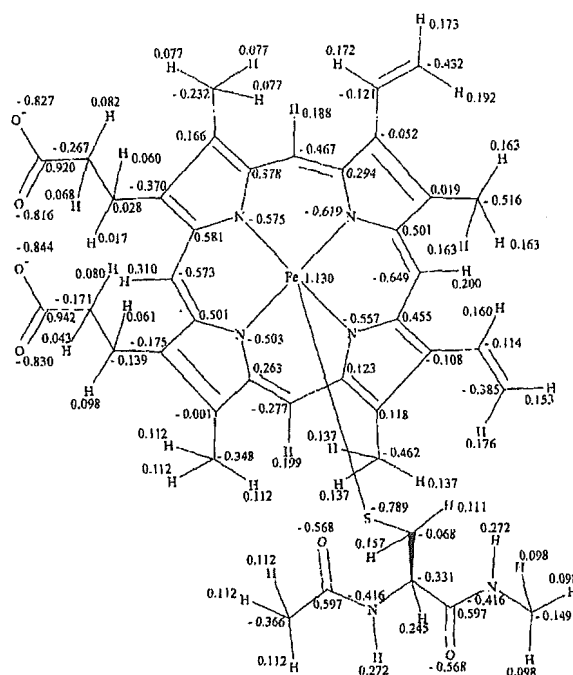

Figure 7. RESP charges calculated for model 1.

and ix, the latter produced more reasonable values for structural features other than those around the iron atom. These results confirm that method ix is applicable when modeling P450s.

The atomic charges for model 1 are illustrated in Figure 7,

Table 3. Optimized Structures for Model 2.

	(a) Bond lengths around Fe/Å												
Method	EXAFS 1	EXAFS 2	X-ray 1	X-ray 2	i	ii	iii	iv	v	vi	vii	viii	ix
Fe—S	2.23	2.30	2.20	2.324	2.242	2.489	2.482	2.434	2.464	2.473	2.358	2.441	2.324
Fe—N	2.06	2.05	2.05	2.064	2.038	2.158	2.163	2.193	2.151	2.143	2.171	2.005	2.094

	(b) Bond angles around Fe/degree									
Method	X-ray 1	X-ray 2	i	ii	iii	iv	v	vi	vii	viii	ix
N_α—Fe—N_α	155.6	155.7	167.0	145.0	144.7	140.3	148.0	149.7	147.1	168.2	153.7
N_α—Fe—N_β	87.4	87.5	89.3	84.8	84.7	83.4	85.7	86.1	85.7	89.4	87.1

	(c) Distances between N_4 plane and Fe/Å									
Method	X-ray 1	X-ray 2	i	ii	iii	iv	v	vi	vii	viii	ix
N_4—Fe	0.43	0.434	0.231	0.648	0.655	0.744	0.591	0.558	0.588	0.206	0.479

Optimized structures using various quantum chemical methods for model 2 compared with experimental results.

(a) Fe-S bond stretching

(b) Fe-S-C angle bending

(c) X-Fe-S-X torsional rotation

(d) Du1-Fe stretching

(e) Du2-Fe-S bending
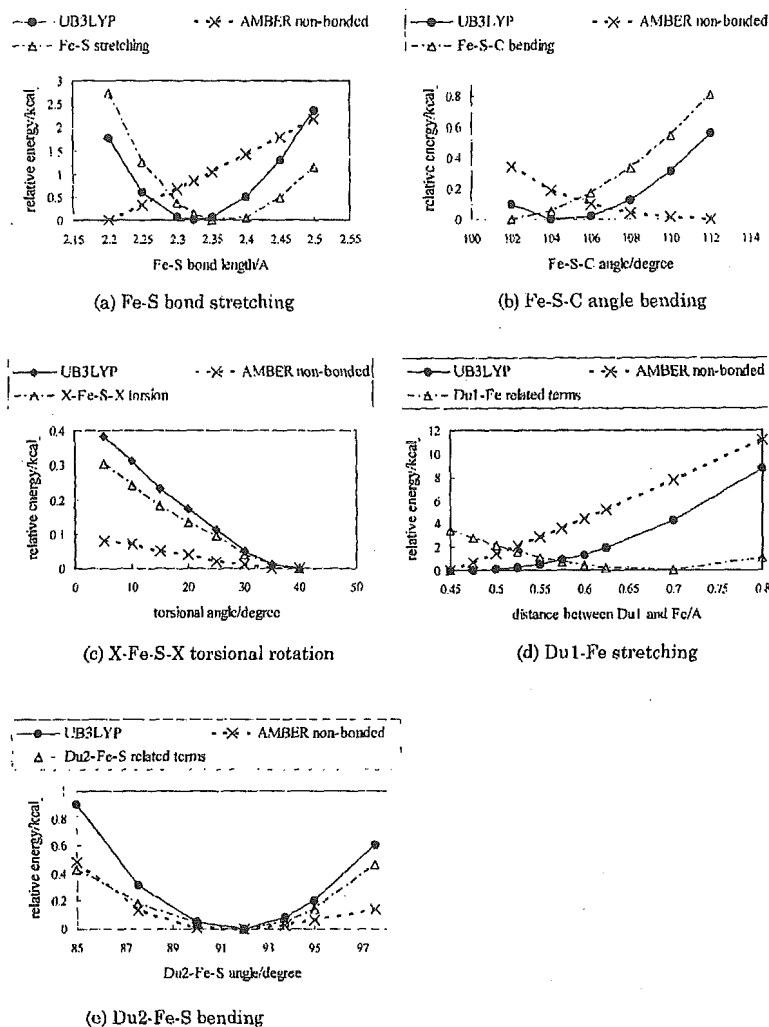
Figure 8. Energy profiles of model 2. The relative value of the energies obtained by UB3LYP (solid line), nonbonded interactions by AMBER force-field (dashed line) and the differences between the solid and the dashed line (alternate long and short dash line) are illustrated.

energy profiles for bond stretching, angle bending, and torsional motion are shown in Figure 8, and the resultant parameters are described in Table 4. The harmonic–oscillator approximations, which play important roles in force fields, cannot be adopted for bond lengths and angles that are far from equilibrium internuclear distances and bond angles. Therefore, energy profiles were obtained between 2.2 and 2.5 Å for Fe—S bond stretching, between 102 and 112° for Fe–S–C angle bending, between 0.45 and 0.80 Å for Du1–Fe stretching, and between 85.0 and 97.5° for Du2–Fe–S bending. The energy profile for X–Fe–S–X torsional motion was calculated between 5 and 40° because of the symmetry of porphyrin. These parameters were calculated to fit the energy differences between the UB3LYP calculations and the nonbonded interactions of the AMBER force field (the alternate long and short dashed

lines in Fig. 8). The values were qualitatively consistent with the atomic charges of other molecules[31] and parameters,[33] and were also quantitatively close to other values. Furthermore, the equilibrium bond length (r_{eq}) of Fe—S and the equilibrium bond angle (θ_{eq}) of Fe–S–C were 2.377 Å and 100.8°, respectively, which is consistent with experimental results.

To validate the calculated atomic charges and parameters, MM calculations of P450cam with five-coordinated Fe(III) were carried out. Figure 9 shows that the structures of heme with the axial ligand Cys357 before (dark gray) and after (light gray) the MM calculations were highly similar—the RMSD was only 0.394 Å. This suggests that the force field parameters determined in this study are consistent with the experimental structure of P450cam. Furthermore, the RMSD for porphyrin and Cys357 (excluding the

Table 4. Parameters Calculated by Energy Profiles of Model 2.

(a) Parameters for bond stretching

	K_r/kcal $(mol\ Å^2)^{-1}$	r_{eq}/Å
Fe—S	87.589	2.377
Fe—N	64.594	2.200

(b) Parameters for angle bending

	K_θ/kcal $(mol\ radian^2)^{-1}$	θ_{eq}/degree
Fe—S—C	21.646	100.8
N_α—Fe—N_α	19.683	135.6
N_α—Fe—N_β	27.911	88.1
N—Fe—S	13.277	92.0
C—N—Fe	47.739	124.3

(c) Parameters for torsional motion around Fe—S bond

	No. of paths	V_n/kcal mol^{-1}	γ/degree	n
X—Fe—S—X	1	0.034	0.0	4.0

side-chain atoms of protoporphyrin IX) was only 0.135 Å. This suggests that the calculated structure around Fe—S is similar to the crystal structure. These results indicate that the RESP charges and the AMBER force field parameters around Fe—S determined in this study are appropriate for use in the modeling of P450s. Further improvements to the MM calculations might be accomplished by refining the parameters around the side-chain atoms of protoporphyrin IX using quantum chemical calculations.

Additional validation of these atomic charges and force-field parameters has already been reported.[42] In ref. 42, homology models of the wild types and mutants of human CYP2C19 and CYP2C9 were constructed, and the structures of these 11 proteins were refined by MM and CMD calculations using the parameters determined in this study. The results of computational docking studies on these models with (S)-mephenytoin, which is one of the specific substrates of CYP2C19, reproduced the experimental enzyme activities without exception. Furthermore, in the calculated three-dimensional structure of the CYP2C19-(S)-mephenytoin complex, the 4'-hydrogen of (S)-mephenytoin was close to the heme iron, which was consistent with the experimentally observed 4'-hydroxylation activity of (S)-mephentyoin. These results suggest that the force field parameters determined in this study, which play significant roles in the construction of models, are reasonable for use in calculations on P450s. Therefore, quantum chemical calculations on model 2 using the UB3LYP method, with the MIDI basis set for iron and the 4-31G* basis set for other elements, appear to be suitable for preparing force field parameters for MM and CMD.

In this study, classical force field parameters of P450s were determined. Although they are useful tools for calculations of

biopolymers, ligand-protein interactions are represented by only van der Waals and Coulombic terms. Static structures of ligand-protein complexes, especially inhibitor-protein complexes, can be predicted and refined in reasonable costs by using classical force field. However, for more detailed analyses of ligand-protein interactions such as enzymatic reaction, which is interesting and important in the dynamic properties of substrate-protein complexes, classical mechanical methods are inadequate because electronic state changes induced by ligand docking play significant roles in these systems. To these purposes, quantum chemical treatment of complexes, for example, QM/MM method or all-electron calculations, are indispensable.

Conclusions

Simplified models are useful if a number of quantum chemical calculations are required on large systems, such as P450s. In this study, an Fe(III) porphyrin with a methylthio group as its axial ligand was used in place of Fe(III) protoporphyrin IX, the axial ligand of which is ACE-CYS-NME. Comparing the results of quantum calculations using various methods suggests that MIDI with Hay's diffuse basis sets are preferable for iron, and that the UB3LYP method is appropriate for high-spin state iron-porphyrin systems with five-coordinated Fe(III). Although the semiempirical AM1 method gave the second-best results after DFT, the structure around the iron atom differed between models 1 and 2. These results might indicate that additional AM1-d parameters for iron do not always work well because the original AM1 method does not include parameters for transition metals. As the AM1 method is highly time-effective, more detailed studies of its strengths and weaknesses are required. We intend to investigate these factors further in a future study.

By using the series of quantum chemical calculations described in this study, atomic charges and force field parameters, which are essential tools of MM and CMD simulations, can be prepared for the study of proteins that include a nonamino acidic molecule. Computer-aided drug design trials, such as de novo design and virtual screening, could be carried out for a wide variety of drug targets using these calculations.
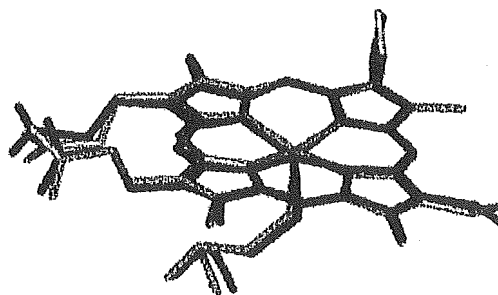

Figure 9. Comparison of the structure of heme and Cys357 before and after minimization (dark and light gray, respectively) using the AMBER force-field with obtained parameters.

References

1. Miller, W. L. Endocr Rev 1988, 9, 295.
2. Capdevila, J.; Chacos, N.; Werringloer, J.; Prough, R. A.; Estabrook, R. W. Proc Natl Acad Sci USA 1981, 78, 5362.
3. Makita, K.; Falck, J. R.; Capdevila, J. H. FASEB J 1996, 10, 1456.
4. Leo, M. A.; Iida, S.; Lieber, C. S. Arch Biochem Biophys 1984, 234, 305.
5. Leo, M. A.; Lasker, J. M.; Raucy, J. L.; Cho-il, K.; Black, M.; Lieber, C. M. Arch Biochem Biophys 1989, 269, 305.
6. Wrighton, S. A.; Stevens, J. C. Crit Rev Toxicol 1992, 22, 1.
7. Guengerich, F. P. J Pharmacokinet Biopharm 1996, 24, 521.
8. Ingelman-Sundberg, M. Trends Pharmacol Sci 2004, 25, 193.
9. Schlighting, I.; Berendzen, J.; Chu, K.; Stock, A. M.; Maves, S. A.; Benson, D. E.; Sweet, R. M.; Ringe, D.; Petsko, G. A.; Sligar, S. G. Science 2000, 287, 1615.
10. Fisher, M. T.; Sligar, S. G. J Am Chem Soc 1985, 107, 5018.
11. Harris, D.; Loew, G.; Waskell, L. J Am Chem Soc 1998, 120, 4308.
12. Harris, D. L.; Loew, G. H. J Am Chem Soc 1998, 120, 8941.
13. Ogliaro, F.; de Visser, S. P.; Cohen, S.; Kaneti, J.; Shaik, S. Chem BioChem 2001, 11, 848.
14. Ogliaro, F.; Filatov, M.; Shaik, S. Eur J Inorg Chem 2000, 2455.
15. de Visser, S. P.; Ogliaro, F.; Harris, N.; Shaik, S. J Am Chem Soc 2001, 123, 3037.
16. Scherlis, D. A.; Cymeryng, C. B.; Estrin, D. A. Inorg Chem 2000, 39, 2352.
17. de Visser, S. P.; Ogliaro, F.; Sharma, P. K.; Shaik, S. J Am Chem Soc 2002, 124, 11809.
18. de Visser, S. P.; Kumar, D.; Cohen, S.; Shacham, R.; Shaik, S. J Am Chem Soc 2004, 126, 8362.
19. de Groot, M. J.; Havenith, R. W. A.; Vinkers, H. M.; Zwaans, R.; Vermeulen, N. P. E.; van Lenthe, J. H. J Comput-Aided Mol Des 1998, 12, 183.
20. Filatov, M.; Harris, N.; Shaik, S. J Chem Soc, Perkin Trans 2 1999, 399.
21. Nakano, T.; Kaminuma, T.; Sato, T.; Akiyama, Y.; Uebayasi, M.; Kitaura, K. Chem Phys Lett 2000, 318, 614.
22. Sato, F.; Shigemitsu, Y.; Okazaki, I.; Yahiro, S.; Fukue, M.; Kozuru, S.; Kashiwagi, H. Int J Quant Chem 1997, 63, 245.
23. Guallar, V.; Friesner, R. A. J Am Chem Soc 2004, 126, 8501.
24. Autenrieth, F.; Tajkhorshid, E.; Baudry, J.; Luthey-Schulten, Z. J Comp Chem 2004, 25, 1613.
25. Tatewaki, H.; Huzinaga, S. J Chem Phys 1980, 72, 339.
26. Hay, P. J. J Chem Phys 1977, 66, 4377.
27. Mulliken, R. S. J Chem Phys 1955, 23, 1833.
28. Breneman, C. M.; Wiberg, K. B. J Comp Chem 1990, 11, 361.
29. Singh, U. C.; Kollman, P. A. J Comp Chem 1984, 5, 129.
30. Bayly, C. I.; Cieplak, P.; Cornell, W. D.; Kollman, P. A. J Phys Chem 1993, 97, 10269.
31. Cieplak, P.; Cornell, W. D.; Bayly, C.; Kollman, P. A. J Comp Chem 1995, 16, 1357.
32. Case, D. A.; Pearlman, D. A.; Caldwell, J. W.; Cheatham, T. E., III; Ross, W. S.; Simmerling, C. L.; Darden, T. A.; Merz, K. M.; Stanton, R. V.; Cheng, A. L.; Vincent, J. J.; Crowley, M.; Tsui, V.; Radmer, R. J.; Duan, Y.; Pitera, J.; Massova, I.; Seibel, G. L.; Singh, U. C.; Weiner P. K.; Kollman, P. A. AMBER 6; University of California: San Francisco, 1999.
33. Cornell, W. D.; Cieplak, P.; Bayly, C. I.; Gould, I. R.; Merz, K. M.; Ferguson, D. M.; Spellmeyer, D. C.; Fox, T.; Caldwell, J. W.; Kollman, P. A. J Am Chem Soc 1995, 117, 5179.
34. Poulos, T. L.; Finzel, B. C.; Howard, A. J. J Mol Biol 1987, 195, 687.
35. SYBYL 6.9.2; Tripos Inc.: St. Louis, 2004.
36. Stewart, J. J. P. MOPAC2002; Fujitsu Limited: Tokyo, 2001.
37. Frisch, M. J.; Trucks, G. W.; Schlegel, H. B.; Scuseria, G. E.; Robb, M. A.; Cheeseman, J. R.; Zakrzewski, V. G.; Montgomery, J. A.; Stratmann, R. E.; Burant, J. C.; Dapprich, S.; Millam, J. M.; Daniels, A. D.; Kudin, K. N.; Strain, M. C.; Farkas, O.; Tomasi, J.; Barone, V.; Cossi, M.; Cammi, R.; Mennucci, B.; Pomelli, C.; Adamo, C.; Clifford, S.; Ochterski, J.; Petersson, G. A.; Ayala, P. Y.; Cui, Q.; Morokuma, K.; Malick, D. K.; Rabuck, A. D.; Raghavachari, K.; Foresman, J. B.; Cioslowski, J.; Ortiz, J. V.; Baboul, A. G.; Stefanov, B. B.; Liu, G.; Liashenko, A.; Piskorz, P.; Komaromi, I.; Gomperts, R.; Martin, R. L.; Fox, D. J.; Keith, T.; Al-Laham, M. A.; Peng, C. Y.; Nanayakkara, A.; Gonzalez, C.; Challacombe, M.; Gill, P. M. W.; Johnson, B. G.; Chen, W.; Wong, M. W.; Andres, J. L.; Head-Gordon, M.; Replogle, E. S.; Pople, J. A. Gaussian 98 Revision A.7; Gaussian, Inc.: Wallingford, 1998.
38. Hahn, J. E.; Hodgson, K. O. J Biol Chem 1982, 257, 10934.
39. Cramer, S. P.; Dawson, J. H.; Hodgson, K. O.; Hager, L. P. J Am Chem Soc 1978, 100, 7282.
40. Tang, S. C.; Koch, S.; Papaefthymiou, G. C.; Foner, S.; Frankel, R. B.; Ibers, J. A.; Holm, R. H. J Am Chem Soc 1976, 98, 2414.
41. Chothia, C.; Lesk, A. M. EMBO J 1986, 5, 823.
42. Oda, A.; Yamaotsu, N.; Hirono S. Pharm Res 2004, 21, 2270.

JOC Note

Convenient Synthesis of Oxazolidinones by the Use of Halomethyloxirane, Primary Amine, and Carbonate Salt

Yumiko Osa, Yuka Hikima, Yoko Sato, Kouichi Takino, Yoshihiro Ida, Shuichi Hirono, and Hiroshi Nagase*

School of Pharmaceutical Sciences, Kitasato University, 5-9-1, Shirokane, Minato-ku, Tokyo 108-8641, Japan

nagaseh@pharm.kitasato-u.ac.jp
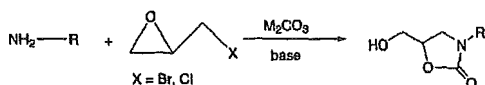
Primary amines reacted with carbonate salts (Na_2CO_3, K_2CO_3, Cs_2CO_3, and Ag_2CO_3) and halomethyloxiranes in the presence of a base such as DBU or TEA to give oxazolidinones in high yields. The use of K_2CO_3 among these carbonate gave the best yield in this synthesis. A reaction mechanism was proposed that the oxazolidinone was obtained from an oxazinanone intermediate via a bicyclo[2.2.1] intermediate. The present reaction can be widely applied to convenient synthesis of useful N-substituted oxazolidinones and chiral oxazolidinones.

Oxazolidinones can be used as the precursors of naturally occurring amino alcohols and amino acids which have been synthesized by a variety of methods.[1] In addition, they are useful as chiral auxiliaries[2] in asymmetric synthesis.[1a] Recently, some oxazolidinone derivatives such as DUP-105,[3] DUP-721,[3] and linezolid (Zyvox)[3b,4] have attracted much interest as monodrug- or multidrug-resistant antibacterial agents.[5] Early synthesis of oxazolidinones was carried out via the reactions of 1,2-amino alcohols and phosgene or its derivatives[6] or amino alcohols with carbon dioxide under high pressure.[7] Recently, carbohydrate derivatives were also used in the synthesis of oxazinanone and oxazolidinone.[8] However, these methods required multiple steps, and the total

SCHEME 1

yields were not always high. As an improved method to overcome the defects, cyclic carbamate synthesis by use of carbon dioxide dissolved in protic solvents containing amines and oxiranes was reported by Toda et al.[9] When primary amines reacted with halomethyloxiranes and a large amount of carbon dioxide under neutral conditions, six-membered cyclic carbamates of oxazinanones were formed.[10] They proposed a reaction mechanism by which the ammonium carbamate intermediate reacted with oxirane. They also used 2-(1-haloalkyl)oxirane and primary amine in the presence of cesium carbonate (Cs_2CO_3) and proposed a mechanism by which carbon dioxide derived from Cs_2CO_3 reacted with the intermediate (2-alkyl-3-aminomethyloxirane) to form oxazolidinone.[11] However, these reactions did not give a high yield of oxazolidinone.

We have recently found a simple method to synthesize oxazolidinone derivatives using primary amine and halomethyloxirane in the presence of various carbonate salts. The reaction is shown in Scheme 1.

At the beginning of our research, we used allylamine (1a, 2 molar equiv), which reacted with halomethyloxirane (2, 2 molar equiv, bromomethyloxirane 2a, and chloromethyloxirane 2b) in the presence of potassium carbonate or silver carbonate (1 molar equiv) in methanol at room temperature to afford oxazolidinone in 45% yield. The structure of N-allyl-5-hydroxymethyloxazolidin-2-one

* To whom correspondence should be addressed. Tel: +81-3-5791-6372. Fax: +81-3-4442-5707.

(1) (a) Ager, D. J.; Prakash, I.; Schaad, D. R. Chem. Rev. 1996, 96, 835–875. (b) Dyen, M. E.; Swern, D. Chem. Rev. 1967, 67, 197–246.

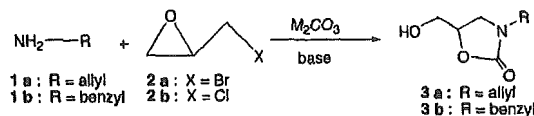(2) (a) Evans, D. A.; Bartroli, J.; Shih, T. L. J. Am. Chem. Soc. 1981, 103, 2127–2129. (b) Evans, D. A. Aldrichim. Acta 1982, 15, 23–32. (c) Evans, D. A.; Takacs, J. M.; McGee, L. R.; Ennis, M. D.; Mathre, D. J.; Bartroli, J. Pure. Appl. Chem. 1981, 53, 1109–1127.

(3) (a) Gregory, W. A.; Brittelli, D. R.; Wang, C.-L. J.; Wuonola, M. A.; McRipley, R. J.; Eustice, D. C.; Eberly, V. S.; Bartholomew, P. T.; Slee, A. M.; Forbes, M. J. Med. Chem. 1989, 32, 1673–1681. (b) Gordeev, M. F. Curr. Opin. Drug Discovery Devel. 2001, 4, 450–461. (c) Slee, A. M.; Wuonola, M. A.; McRipley, R. J.; Zajac, I.; Zawada, M. J.; Bartholomew, P. T.; Gregory, W. A.; Forbes, M. Antimicrob. Agents Chemothr. 1987, 31, 1791–1797.

(4) (a) Bolmstrom, A.; Ballow, C. H.; Qwarnstrom, A.; Biedenbach, D. J.; Jones, R. N. Clin. Microbiol. Infec. 2002, 8, 791–800. (b) Barbachyn, M. R.; Ford, C. W. Angew. Chem., Int. Ed. 2003, 42, 2010–2023. (c) Wang, G.; Hollingsworth, R. I. Tetrahedron: Asymmetry 2000, 11, 4429–4432.

(5) Barbachyn, M. R.; Toops, D. S.; Grega, K. C.; Hendges, S. K.; Ford, C. W.; Zurenko, G. E.; Hamel, J. C.; Shaadt, R. D.; Stapert, D.; Yagi, B. H.; Buysse, J. M.; Demyan, W. F.; Kilburn, J. O.; Glickman, S. E. Bioorg. Med. Chem. Lett. 1996, 6, 1009–1014.

(6) (a) Newman, M. S.; Kutner, A. J. J. Am. Chem. Soc. 1951, 73, 4199–4204. (b) Lubell, W.; Rapoport, H. J. Org. Chem. 1989, 54, 3824–3831. (c) Bonner, M. P.; Thornton, E. R. J. Am. Chem. Soc. 1991, 113, 1299–1308. (d) Palomo, C.; Berree, F.; Lindent, A.; Villalgordo, J. M. J. Chem. Soc., Chem. Commun. 1994, 1861–1862. (e) Efskind, J.; Romming, C.; Undheim, K. J. Chem. Soc., Perkin Trans. 1 1999, 1677–1684.

(7) (a) Lynn. J. W. U. S. Patent 2,975,187, 1961; Chem. Abstr. 1961, 55, 16568. (b) Steele, A. B. U. S. Patent 2,868,801, 1959; Chem. Abstr. 1959, 53, 10261.

(8) (a) Hu, N. X.; Aso, Y.; Otsubo, T.; Ogura, F. J. Chem. Soc., Chem. Commun. 1987, 1447–1448. (b) Lewis, N.; McKillop, A.; Taylor, R. J. K.; Watson, R. J. Synth. Commun. 1995, 25, 561–568. (c) Li, G.; Lenington, S.; Willis, S.; Kim, S. H. J. Chem. Soc., Perkin Trans. 1 1998, 1753–1754. (d) Feroci, M.; Inesi, A.; Mucciante, V.; Rossi, L. Tetrahedron Lett. 1999, 40, 6059–6060. (d) Tanimori, S.; Kirihata, M. Tetrahedron Lett. 2000, 41, 6785–6788. (e) Casadei, M. A.; Feroci, M.; Inesi, A.; Rossi, L.; Sotgiu, G. J. Org. Chem. 2000, 65, 4759–4761. (f) Caggiano, L.; Davies, J.; Fox, D. J.; Moody, D. C.; Warren, S. Chem. Commun. 2003, 1650–1651. (g) Dinsmore, C. J.; Mercer, S. P. Org. Lett. 2004, 6, 2885–2888. (i) Ella-Menye, J.-R.; Sharma, V.; Wang, G. J. Org. Chem. 2005, 70, 463–469.

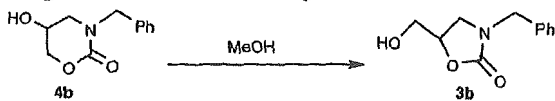(9) (a) Toda, T. Chem. Lett. 1977, 957–958. (b) Saito, N.; Hatakeda, K.; Ito, S.; Asano, T.; Toda, T. Heterocycles 1981, 15, 905–906. (c) Toda, T. Nippon Kagaku Kaishi 1982, 2, 282–288. (d) Saito, N.; Hatakeda, K.; Ito, S.; Asano, T.; Toda, T. Bull. Chem. Soc. Jpn. 1986, 59, 1629–1631. (e) Toda, T.; Kitagawa, Y. Angew. Chem., Int. Ed. Engl. 1987, 26, 334–335. (f) Saito, N.; Hatakeda, K.; Ito, S.; Asano, T.; Namai, Y.; Toda, T. Agric. Biol. Chem. 1987, 51, 1193–1194.

(10) (a) Asano, T.; Saito, N.; Ito, S.; Hatakeda, K.; Toda, T. Chem. Lett. 1978, 311–312. (b) Saito, N.; Hatakeda, K.; Ito, S.; Asano, T.; Toda, T. Nippon Kagaku Kaishi 1986, 9, 1196–1201.

(11) Yoshida, M.; Ohshima, M.; Toda, T. Heterocycles 1993, 35, 623–626.

TABLE 1. Conversion Conditions of Six-Membered Ring 4b to Five-Membered Ring 3b

	molar ratio				yield (%)	
run[a]	4b/1b[b]/ K₂CO₃/base	base (equiv)	reaction		3b	recovery 4b
1	1:0:0:0		reflux, o.n.[c]			100
2	2:2:1:0		rt, stirring, o.n.		94	
3	2:2:1:0		reflux, 2 hr		quant	
4	1:0:0:5	DBU	reflux, 5.5 hr		96	
5	1:0:0:5	TEA	reflux, o.n.			100
6	1:0:0:4	TEA (3), DBU (1)	reflux, o.n.		quant.	

[a] All reactions were carried out in MeOH. [b] 1b = NH₂CH₂-Ph. [c] o.n. = overnight.

(3a) obtained from allylamine (1a) was determined, in detail, using ¹H NMR, ¹³C NMR, ¹H–¹H decoupling, NOE, and LSPD[12] and also was supported by X-ray analysis.[13] Furthermore, it was confirmed that the carbon of the carbonate salt was introduced at the 2-position in 3a by the reaction using isotopic Ag₂¹³CO₃ (98% atomic purity of ¹³C) instead of K₂CO₃.

To elucidate the reaction mechanism and increase the yields, the IR spectrum of the reaction mixture, which was obtained by the reaction of molar ratios of K₂CO₃ (1 mol), benzylamine (instead of allylamine because of its high boiling point compared with that of allylamine), and bromomethyloxirane (2 mol) in methanol at 0 °C, was measured. We found the bands at 1680 and 1730 cm⁻¹ in the reaction mixture. The former band is assigned[14] to a six-membered cyclic carbamate of oxazinanone, which was also reported by Toda et al.[9e] The latter band corresponds to a five-membered cyclic carbamate of oxazolidinone. The spot of oxazinanone in TLC (the value of R_f was 0.47; chloroform/methanol = 10:1) diminished with the reaction time. On the other hand, the spot of oxazolidinone in TLC (the value of R_f was 0.58; chloroform/methanol = 10:1) enlarged with the reaction time. These facts support that oxazinanone is an unstable intermediate (kinetic product) in the reaction.

For further confirmation of oxazinanone formation in the reaction process, the isomerization of N-benzyl-5-hydroxyoxazinanone (4b) to N-benzyl-5-hydroxymethyl-oxazolidinone (3b) was examined as shown in Table 1. When only 4b was refluxed in methanol, 3b was not obtained and 4b was recovered (run 1). On the other hand, the reaction conditions (even if at room temperature) for oxazolidinone synthesis in the presence of K₂CO₃ gave 3b in 94% yield (run 2). These facts showed that K₂CO₃ is necessary for the conversion of 4b to 3b. Furthermore, under reflux for 2 h, 3b was obtained quantitatively (run 3). The use of DBU instead of K₂CO₃

also gave 3b in 96% yield (run 4), but by the use of TEA instead of K₂CO₃ 4b was quantitatively recovered (run 5). When 1 equiv of DBU was added after addition of 3 equiv of TEA to the reaction solution, 3b was obtained in quantitative yield (run 6). The above results showed that the ring contraction reaction from six-membered cyclic carbamate to five-membered cyclic carbamate perfectly proceeded in the presence of K₂CO₃ or DBU but did not occur in the presence of only TEA. These results mean that a strong base or a basic condition is necessary to form 3b.

Furthermore, total molecular energy calculation of compounds 3b and 4b was carried out by the use of Merck Molecular Force Field (MMFF94).[15] The total energy of 3b is 31.2 kcal/mol and that of 4b is 34.1 kcal/mol. Therefore, the calculation result shows that oxazolidinone is more stable than oxazinanone. This result also supports that the six-membered ring is an intermediate of the reaction process. Wang et al. also reported six-membered ring oxazinanone was converted to more stable 5-membered ring oxazolidinone under base conditions and heating,[8i] which gave supporting evidence in our present conversion.

Based on the above discussion, a reaction mechanism is proposed as depicted in Scheme 2. Two routes (I and II) are supposed to form an intermediate D. In route I, first, primary amine 1 attacks the C–X bond of halomethyloxirane 2 to afford an intermediate A. Subsequently, a carbonate ion attacks A to form the intermediate D. In route II, 1 attaches the oxirane ring of 2 to give intermediate B. As oxirane ring 2 may be more electrophilic than the C–X bond in the case of an attack of the alkoxide ion,[16] a first attack of amine 1 to the oxirane ring may be reasonably considered.[16,17] Subsequently, the resulting alkoxide ion of intermediate B attacks the carbon atom of the halomethyl group to form C. Next, the carbonate ion attacks the oxirane ring C to afford the intermediate D. Then the resulting amino nitrogen attacks the carbonyl group in D to cyclize intramolecularly to a six-membered ring of oxazinanone (4). In the mechanism, the intermediate D can cyclize only to six-membered oxazinanone, not five-membered oxazolidinone. Two routes III and IV are considered as the conversion process of oxazolidinone (3) from compound 4. In route III, the alkoxide ion in intermediate E under strong basic condition attacks intramolecularly the carbonyl carbon to give a bicyclo[2.2.1] intermediate F, which is subsequently converted to a five-membered ring of oxazolidinone 3. In route IV, a methoxide ion generated from methanol under strong basic condition attacks the carbonyl carbon of the oxazinanone (intermediate G) to open a ring structure. The resulting alkoxide ion (intramolecularly) attacks the carbon of intermediate H to form compound 3. However, it is considered that the intramolecular attack in route III may be more favorable (entropy) than the intermolecular one of the methoxide

(12) (a) Takeuchi, S.; Uzawa, J.; Seto, H.; Yonehara, H, *Tetrahedron Lett.* 1977, 34, 2943–2946. (b) Seto, H.; Sasaki. T.; Yonehara, H.; Uzawa, J. *Tetrahedron Lett.* 1978, 10, 923–926. (c) LSPD (long range selective proton decouple) was used to detect the ring protons adjacent to the oxygen and nitrogen atoms linked to carbonyl carbon.

(13) Osa, Y.; Sato, Y.; Hatano, A.; Takeda, K.; Takino, K.; Takayanagi, H. *Anal. Sci.* 2003, 19, x17–x18.

(14) *The Aldrich Library of FT-IR Spectra*, Edition II; Aldrich: Milwaukee, 1997.

(15) (a) Halgren, T. A. *J. Am. Chem. Soc.*, 1992, 114, 7827–7843. (b) Halgren, T. A. *J. Comput. Chem.* 1996, 17, 490–519.

(16) Clayden, J.; Greeves, N.; Warren, S.; Wothers, P. *Organic Chemistry*; Oxford University Press: Oxford, 2001.

(17) The textbook of organic chemistry (for example, the book written by Warren[16]) described the oxirane ring of epichlorohydrin is more electrophilic than the C–Cl bond with alkoxide. Therefore, the carbonate ion was reacted with the oxirane ring of epibromohydrin.

SCHEME 2
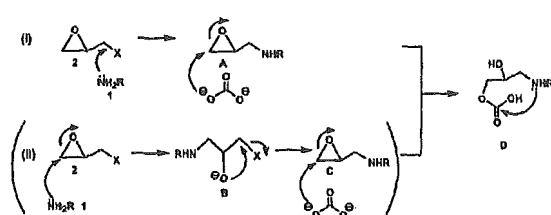
SCHEME 3
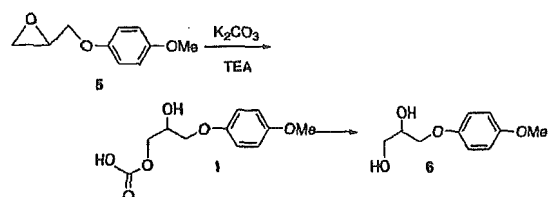
ion in route IV. Therefore, we think route III may be more reasonable. Compound 4 will be formed as a kinetic product and 3 can be obtained as a thermodynamic product.

The difference between our mechanism and that of Toda was mainly the reaction intermediate. In the Toda mechanism,[11] the carbamate anion was formed by reacting 2-(1-haloalkyl)oxirane and amine with CO_2 derived from Cs_2CO_3 to open the epoxide in the alkaline medium and the resulting alkoxide ion attacks at the C–X carbon to give an epoxy ring. However, as carbonate (Cs_2CO_3) could not be converted to CO_2 under the strong basic condition using CsOH, CO_2 could not be produced to form the carbamate ion. In our mechanism, the carbonate ion, not the carbamate anion, attacks the halomethyloxirane directly.

Furthermore, the reactivity (nucleophilicity) of the carbonate ion was confirmed by the reaction of 2,3-epoxypropyl 4-methoxyphenyl ether (5) and K_2CO_3. Though the reaction of 5 and K_2CO_3 (dried in vacuo at 120 °C for 10 h) in anhydrous DMF gave no products under the anhydrous condition, the addition of TEA to the solution containing 5 and K_2CO_3 in anhydrous DMF under anhydrous condition afforded a diol (6) which was obtained by hydrolysis of the carbonate intermediate I in 43% yield[18] (Scheme 3). The preparation of the product, diol (6), suggests attack of the carbonate ion to oxirane in the presence of a base.

On the basis of the above proposed reaction mechanism as shown in Scheme 2, we examined optimization of the reaction conditions. In Scheme 2, the excess of reagents for primary amine was expected to increase the yields, and strong basic condition would be needed for formation for the alkoxide ion to attack the carbonyl carbon (E, F) and reflux condition would be able to convert the six-membered ring, oxazinanone, to the five-membered ring, oxazolidinone, easily. Table 2 shows various conditions to optimize various molar ratios of the reagents and temperature. The high yield of N-benzyl-5-hydroxy-
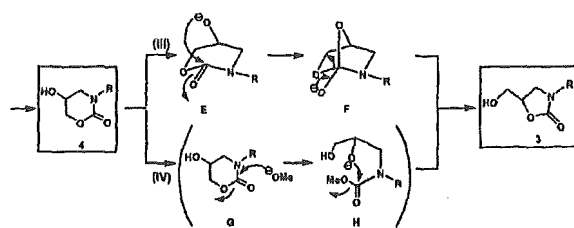
TABLE 2. Reaction Conditions for Synthesis of 3b

		molar ratio		yield of
run	X	1b/2/K_2CO_3/TEA	reaction	3b (%)
1	Br	1:1:1:1	rt, o.n.[a]	28
2	Br	1:1:1:1	reflux, o.n.	37
3	Br	1:2:2:2	rt, o.n.	29
4	Br	1:3:1:1	rt, o.n.	61
5	Br	1:5:5:5	rt, o.n.	68
6	Br	1:5:5:0	reflux, o.n.	76
7	Br	1:5:5:5	reflux, o.n.	83
8	Br	1:10:10:10	rt, o.n.	58
9	Br	1:10:10:10	reflux, o.n.	88
10	Cl	1:5:5:5	reflux, o.n.	81

[a] o.n. = overnight.

methyloxazolidin-2-one (3b) (more than 80% yield) was obtained under the conditions of a large mole ratio (more than 5 molar equiv) of halomethyloxirane, K_2CO_3 in methanol in the presence of more than 5 mol base (TEA; triethylamine or DBU; 1,8-diazabicyclo[5.4.0]undec-7-ene) per mole of amine under reflux (runs 7, 9, and 10).

The use of one molar ratio of 1b, 1 or 2 molar ratio of 2b, K_2CO_3, and TEA gave a low yield of 3b (runs 1 and 3), and the yield of 3b did not increase even under reflux (37%, run 2). Excess amounts (5 or 10 molar ratios) of 2a, K_2CO_3, and TEA to benzylamine 1b at room temperature gave 3b in 68% and 58% yields (runs 5 and 8) and the yields increased to 83 and 88% under reflux (runs 7 and 9). In the absence of TEA as a base, the yield of 3b was lower than that in run 7 (run 6). It suggested that the addition of a strong base increased the yield of 3b in comparison between runs 6 and 7. The use of chloromethyloxirane 2b instead of bromomethyloxirane 2a gave almost the same yield of 3b (81% yields in the case of 2b (run 10) and 83% in the case of 2a (run 7)). Thus, we were able to optimize the reaction conditions for oxazolidinones on the basis of our reaction mechanism. Pure product 3 was rationally identified on the basis of IR, NMR, elemental analysis, and mass spectra.

Several kinds of carbonate salts were examined to obtain 3 as shown in Table 3. Na_2CO_3, Cs_2CO_3, and Ag_2CO_3 (runs 2, 4, and 6) gave more than 75% yields of 3b.

At the beginning of our study,[19] we examined various primary amines of propyl, isopropyl, n-butyl, heptyl, and cyclohexyl groups. When the reaction conditions of pri-

(18) Tanzer, W.; Muller, H.; Wintzer, J.; Fedtke, M. *Makromol. Chem.* 1987, *188*, 2857–2863.

(19) Osa, Y.; Sato, Y.; Oshimoto, M.; Takino, K.; Takeda, A.; Takayanagi, H. 44th Symposium of J. Synth. Org. Chem., Jpn, Kanto Branch, Niigata, 2002, Abstract pp 123–124.

TABLE 3. The Yield of 3b Using Various Carbonate Salts

PhCH₂-NH₂ · (epoxide)/Br →[M₂CO₃ / TEA][MeOH] HO~~~N-CH₂Ph (oxazolidinone)
1b **2a** **3b**
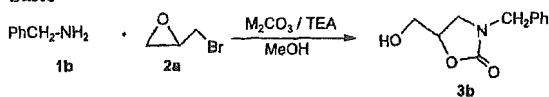
run[a]	M₂CO₃	molar ratio 1b/2a/ M₂CO₃/TEA	reaction	yield of 3b (%)
1	K₂CO₃	1:5:5:5	reflux, under Ar, o.n.[b]	83
2	Na₂CO₃	1:5:5:5	reflux, under Ar, o.n.	77
3	Rb₂CO₃	1:5:5:5	reflux, under Ar, o.n.	28
4	Cs₂CO₃	1:5:5:5	reflux, under Ar, o.n.	82
5	Li₂CO₃	1:5:5:5	reflux, under Ar, o.n.	25
6	Ag₂CO₃	1:5:5:5	reflux, dark, under Ar, o.n.	75

[a] All reactions were carried out in MeOH. [b] o.n. = overnight.

FIGURE 1.

SCHEME 4

NH₂CH₂-⟨benzene⟩-R + (epoxide)/Cl →[K₂CO₃][TEA] HO~~~N-⟨benzene⟩-R

1b: R = H
1c: R = Br
7
8: R = H (80%)
9: R = Br (82%)
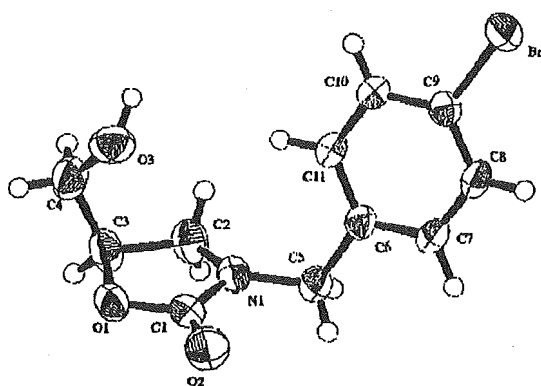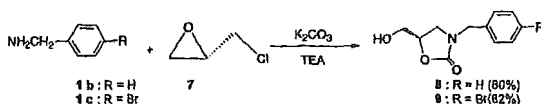
mary amine 1 (2 equiv), bromomethyloxirane 2a (2 equiv), and Ag₂CO₃ or K₂CO₃ (1 equiv) in methanol stirring overnight at room temperature were used, 36–50% yields of the corresponding oxazolidinones were obtained based on each amine. Application of similar optimum reaction conditions to benzylamine will give higher yield of oxazolidinones. The use of aniline as aromatic amine is now under study.

We also applied chiral halomethyloxirane to a synthesis for chiral oxazolidinones to confirm which route the reaction selected, I or II. The reactions of (S)-chloromethyloxirane (7) with benzylamine (1b) and p-bromobenzylamine (1c) under similar conditions to the above method to give oxazolidinones 8 and 9 were carried out (Scheme 4). The stereo structure of N-(p-bromobenzyl)-5-hydroxymethyloxazolidin-2-one (9) was confirmed by means of X-ray analysis (Figure 1).[20] In this reaction, the S-configuration of the oxirane ring inverted to the R-configuration at the 5-position of the oxazolidinone

(20) X-ray data was deposited in the Cambridge Crystallographic Data Centre in CIF format as CCDC 269747 for 9.

nucleus (Scheme 4). The results support route I in the reaction mechanism (Scheme 2) because route II will retain the S-configuration to give S-oxazolidinone in the use of S-chloromethyloxirane. Accordingly, the synthesis of oxazolidinone is supposed to proceed via route I.

In conclusion, the present synthetic method is characterized by a simple procedure, mild reaction conditions, high reaction yield, and high selectivity and will be useful to produce various kinds of N-substituted-5-hydroxymethyloxazolidin-2-one and chiral oxazolidinone. The five-membered ring compound, oxazolidinone, is more stable than the six-membered ring compound, oxazinanone.

Experimental Section

General Procedure for Oxazolidinone. Primary amine (1 mmol ratio) was added to methanol (5 mL) containing an excess amount of halomethyloxirane (5 or 10 mmol ratio), K₂CO₃ (5 or 10 mmol ratio), and TEA (5 or 10 mmol ratio) under reflux overnight. After the solution was cooled to room temperature, the reaction mixture was filtered for removing the solidified, unreacted carbonate salts. Then, the organic layer was evaporated and the residue was solved in AcOEt. The organic layer was washed with NaCl aq and dried using Na₂SO₄. The solvent was evaporated in vacuo. The residue was isolated by silica gel column chromatography with chloroform/methanol (10:1).

N-Benzyl-5-hydroxymethyloxazolidin-2-one (3b): yield 88% as a pale yellow solid; mp 69–70 °C; IR (film) 3200–3620, 1730 cm⁻¹; ¹H NMR (600 MHz, CDCl₃) δ 3.32 (1H, dd, J = 6.5, 8.0 Hz), 3.44 (1H, dd, J = 8.0. 10.0 Hz), 3.62 (1H, dd, J = 13.0, 4.0 Hz), 3.85 (1H, dd, J = 13.0, 3.0 Hz), 4.38, 4.48 (d, 1H, J = 15.0 Hz), 4.58 (1H, m, J = 6.5, 10.0, 4.0, 3.0 Hz), 7.25–7.38 (5H, m); ¹³C NMR (150 MHz, CDCl₃) δ 45.1, 47.9, 62.6, 73.5, 127.7, 127.8, 128.6, 135.4, 156.2; MS (FAB) m/z 208 (M + H)⁺. Anal. Calcd for C₁₁H₁₃NO₃: C, 63.76; H, 6.32; N, 6.76. Found: C, 63.59; H, 6.32; N, 7.01.

N-Benzyl-5-hydroxyoxazinan-2-one (4b). To a methanol (4 mL) solution of bromomethyloxirane 2a (171 μL, 2.0 mmol) was added benzylamine (218 μL, 2.0 mmol). The reaction mixture was bubbled through CO₂ for 5 h and stirred overnight. The reaction mixture was evaporated in vacuo, and then the yellow residue was purified by silica gel column chromatography with chloroform/ethyl acetate (5:1) to give the pure product 4b (163 mg, 39% unoptimized yield) as a pale yellow solid; mp 114–115 °C; IR (KBr) 3200–3620, 1678 cm⁻¹; ¹H NMR (600 MHz, CDCl₃) δ 3.17 (1H, ddd, J = 12.0, 3.0 Hz), 3.38 (1H, dd, J = 12.0, 4.0 Hz), 4.10 (1H, m), 4.20 (1H, dd, J = 3.0, 12.0 Hz), 4.23 (1H, dd, J = 2.5, 12.0 Hz), 4.43, 4.61 (1H, d, J = 15.0 Hz), 7.24–7.32 (5H, m); ¹³C NMR (150 MHz, CDCl₃) δ 51.4, 52.7, 61.2, 70.5, 127.8, 128.1, 128.8, 136.2, 153.5; MS (EI) m/z 207 (M)⁺. Anal. Calcd for C₁₁H₁₃NO₃: C, 63.76; H, 6.32; N, 6.76. Found: C, 63.62; H, 6.41; N, 6.44.

(R)-N-(p-Bromobenzyl)-5-hydroxymethyloxazolidin-2-one (9). p-Bromobenzylamine hydrochloride 1c (100 mg, 0.45 mmol) was removed by washing with NaOH aq: yield 82% as prisms; mp 109–110 °C (crystallized from ethyl acetate); [α]²¹_D = −12.5 (c 0.933, MeOH); IR (film) 3200–3620, 1729 cm⁻¹; ¹H NMR (600 MHz, CDCl₃) δ 3.32 (1H, dd, J = 7.0, 8.0 Hz), 3.40 (1H, dd, J = 8.0. 10.0 Hz), 3.57 (1H, dd, J = 12.0, 4.0 Hz), 3.83 (1H, dd, J = 12.0, 5.0 Hz), 4.32, 4.37 (1H, d, J = 15.0 Hz), 4.55 (1H, dt, J = 10.0, 7.0, 5.0, 4.0 Hz), 7.13, 7.45 (1H, d, J = 8.0 Hz); ¹³C NMR (150 MHz, CDCl₃) δ 45.0, 47.7, 62.9, 73.5, 121.9, 129.7, 131.9, 134.6, 157.9; MS (FAB) m/z 285, 287 (M)⁺. Anal. Calcd for C₁₁H₁₂NO₃Br: C, 46.18; H, 4.23; N, 4.90. Found: C, 46.16; H, 4.28; N, 5.09.

HYDROLYSIS OF ANGIOTENSIN II RECEPTOR BLOCKER PRODRUG OLMESARTAN MEDOXOMIL BY HUMAN SERUM ALBUMIN AND IDENTIFICATION OF ITS CATALYTIC ACTIVE SITES

Shen-Feng Ma, Makoto Anraku, Yasunori Iwao, Keishi Yamasaki, Ulrich Kragh-Hansen, Noriyuki Yamaotsu, Shuichi Hirono, Toshihiko Ikeda, and Masaki Otagiri

Graduate School of Pharmaceutical Sciences, Kumamoto University, Kumamoto, Japan (S.-F.M., M.A., Y.I., M.O.); Department of Pharmacy, Miyazaki Medical College Hospital, Miyazaki, Japan (K.Y.); Department of Medical Biochemistry, University of Aarhus, Aarhus, Denmark (U.K.-H.); the School of Pharmaceutical Sciences, Kitasato University, Tokyo, Japan (N.Y., S.H.); and Drug Metabolism and Pharmacokinetics Research Laboratories, Sankyo Co., Ltd., Tokyo, Japan (T.I.)

ABSTRACT:

In the present study, we investigated the esterase-like activity of human serum albumin (HSA) and the mechanism by which it hydrolyzes, and thereby activates, olmesartan medoxomil (CS-866), a novel angiotensin II receptor antagonist. CS-866 has previously been shown to be rapidly hydrolyzed in serum in which HSA appeared to play the most important role in catalyzing the hydrolysis. We found that the hydrolysis of CS-866 by HSA followed Michaelis-Menten kinetics. Compared with the release of p-nitrophenol from p-nitrophenyl acetate (PNPA), CS-866 showed lower affinity to HSA and a lower catalytic rate of hydrolysis. Thermodynamic data indicated that PNPA has a smaller value of activation entropy (ΔS) than CS-866; consequently, PNPA is more reactive than CS-866. Ibuprofen and warfarin acted as competitive inhibitors of hydrolysis of CS-866, whereas dansyl-L-asparagine, n-butyl p-aminobenzoate, and diazepam did not. These findings suggest that the hydrolytic activity is associated to parts of site I and site II for ligand binding. All chemically modified HSA derivatives (Tyr-, Lys-, His-, and Trp-modifications) had significantly lower reactivity than native HSA; Lys-HSA and Trp-HSA had especially low reactivity. All the mutant HSAs tested (K199A, W214A, and Y411A) exhibited a significant decrease in reactivity, suggesting that Lys-199, Trp-214, and Tyr-411 play important roles in the hydrolysis. Results obtained using a computer docking model are in agreement with the experimental results, and strongly support the hypotheses that we derived from the experiments.

Ester prodrugs are hydrolyzed to their pharmacologically active metabolites after absorption. Esterases present in the small intestine, plasma, and liver are involved in this process. In most cases, intestinal esterases serve as the major enzymes in activation of prodrugs during the first pass through the gut after absorption. However, prodrugs that are relatively resistant to hydrolysis by intestinal esterases enter the blood circulation and are activated by serum (plasma) and liver esterases. The major hydrolyzing enzymes in serum are cholinesterase, arylesterase, carboxylesterase, and albumin. The relative importance of each serum esterase in prodrug activation varies among animal species and prodrugs.

Olmesartan medoxomil [CS-866: (5-methyl-2-oxo-1,3-dioxolen-4-yl) methoxy-4-(1-hydroxyl-1-methylethyl)-2-propyl-1-[4-[2-(tetra-zol-5-yl)-phenyl]phenyl]methylimi-dazol-5-carboxylate] is a novel nonpeptide angiotensin II receptor antagonist that acts as an antihypertensive prodrug (Koike et al., 2001; Neutel, 2001; Brousil and Burke, 2003). After oral administration, CS-866 is rapidly de-esterified, producing an active acid metabolite, olmesartan (RNH-6270) (Fig. 1) (Koike et al., 2001; Neutel, 2001; Brousil and Burke, 2003). Hydrolysis of CS-866 in serum has been observed in several species, and comparison among five species has shown that hydrolytic activity is highest in rabbits, followed by dogs, mice, rats, and humans (Ikeda, 2000). Furthermore, it was found that differences in hydrolytic activity due to serum albumin are large compared to the combined activity of all serum components. Thus, HSA might make an important contribution to activation of CS-866 after oral administration.

In the present study, we examined the esterase-like activity of HSA and the mechanism of its hydrolysis of CS-866. First, the general properties of the hydrolytic reaction of HSA with CS-866 were determined, including the kinetics and thermodynamics, and compared with those of the hydrolytic reaction between HSA and p-nitrophenyl acetate (PNPA) (Means and Bender, 1975; Sakurai et al., 2004). Second, to characterize the effects of exogenous compounds on hydrolysis, we investigated changes in hydrolytic activity in the

Olmesartan medoxomil
CS-866

Ester prodrug

Olmesartan
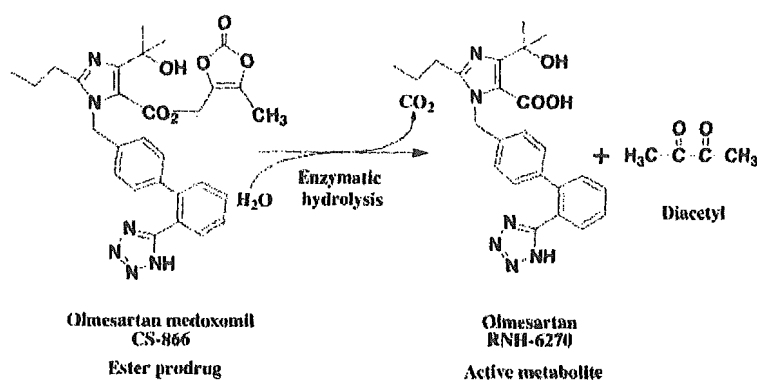RNH-6270

Active metabolite

Fig. 1. Hydrolysis of CS-866 to RNH-6270

presence and absence of various ligands. Then, we examined the importance of certain types of amino acid residues of HSA for the hydrolysis of CS-866, using chemical modification techniques. Recombinant HSA (rHSA) proteins with alterations of specific amino acid residues were prepared using site-directed mutagenesis techniques, to obtain detailed information about the contribution of those residues. Finally, computer docking models of CS-866 and HSA were constructed and were found to be consistent with the experimental results.

Materials and Methods

Materials. HSA was donated by the Chemo-Sera-Therapeutic Research Institute (Kumamoto, Japan). HSA was defatted before use (Chen, 1967).

CS-866 and RNH-6270 were donated by Sankyo Co., Ltd. (Tokyo, Japan). PNPA, succinic anhydride and n-butyl p-aminobenzoate (n-butyl p-AB) were purchased form Nakalai Tesque (Kyoto, Japan). Warfarin was obtained from Eisai Co. (Tokyo, Japan), ibuprofen was obtained from Kaken Pharmaceutical Co. (Osaka, Japan), diazepam was obtained from Sumitomo Pharmaceutical Co. (Osaka, Japan), tetranitromethane was obtained from Aldrich Chemical Co. (Milwaukee, WI), and trinitrobenzenesulfonic acid was obtained from Wako Pure Chemical Industries, Ltd. (Osaka, Japan). Dansyl-L-asparagine (DNSA). 2-hydroxyl-5-nitrobenzyl bromide, and diethyl pyrocarbonate were purchased from Sigma-Aldrich (St. Louis, MO). Restriction enzymes, T4 polynucleotide kinase, calf intestinal alkaline phosphatase, a DNA ligation kit, TaKaRa EX TaqDNA polymerase, and a site-directed mutagenesis kit (oligonucleotide-directed dual amber method) were obtained from Takara Shuzo Co., Ltd. (Kyoto, Japan). A DNA sequence kit was obtained from Applied Biosystems (Tokyo, Japan). The Pichia Expression kit was purchased from Invitrogen (Carlsbad, CA). All other chemicals were of analytical grade.

Esterase-Like Activity Measurement. Procedures for Michaelis-Menten Equation Runs. The reaction was started by adding CS-866 in 100% acetonitrile (5 μl) to preincubated HSA (120 μl, 75 μM), at a final concentration of 10 to 250 μM. Incubation proceeded for 10 min and was terminated by adding 500 μl of acetonitrile to the incubation mixture. We have checked that 4% acetonitrile has little effect on the reaction. After centrifugation for 1 min, a 30-μl aliquot of the deproteinized supernatant was subjected to high-performance liquid chromatography, and RNH-6270 was separated from CS-866 on an ODS column using the following conditions: column, YMC-Pack ODS-AM, AM-302, 150 × 4.6 mm i.d.; column temperature, 40°C maintained by a Hitachi 655A-52 column oven: a Hitachi L-6000 pump; a Hitachi FL detector L-7480 fluorescent monitor; a HITACHI D-2500 Chromato-Integrator; mobile phase, acetonitrile/water/acetic acid, 40:60:0.1; wavelength, excitation = 260 nm, emission = 370 nm; flow rate, 1.0 ml/min.

The reaction between CS-866 and HSA took place at 4°C. Under that condition, Michaelis-Menten equation analysis can be applied,

$$v = \frac{V_{max}[S]}{K_M + [S]}$$ (1)

Here, [S] is the concentration of substrate. That is the case, because previous studies have revealed a linear relationship between $1/V$ and $1/S$ when plotted in a Lineweaver-Burk plot (Koike et al., 2001):

$$\frac{1}{v} = \frac{1}{V_{max}} + \frac{K_M}{V_{max}[S]}$$ (2)

Procedures for Kinetic Runs. Hydrolysis of CS-866 (5 μM) by HSA (at least a 5-fold excess concentration over the substrate) was performed using conditions able to avoid complications due to multiple reactive sites of albumin. Under such conditions, pseudofirst-order rate constant analysis can be performed. The pseudofirst-order rate constant for the release of RNH-6270 (k_{obs}), the dissociation constant of the substrate-HSA complex (K_S), and the catalytic rate constants (k_{cat}) were calculated as reported elsewhere (Sakurai et al., 2004).

Thermodynamic Analysis. Thermodynamic analysis of the HSA-catalyzed reaction was performed at temperatures ranging from 20°C to 40°C. We calculated the thermodynamic parameters, the free energy change for the initial reaction between enzyme and substrate (ΔG_S), the activation free energy for the rate-determining step (ΔG), the free energy difference for the reaction (ΔG_T), the activation energy (E_a), the activation enthalpy change (ΔH), and the activation entropy change (ΔS), using previously published methods (Sakurai et al., 2004).

Effects of Ligands. HSA (120 μl, 75 μM) was preincubated, and the enzymatic reaction was started by adding CS-866 in 100% acetonitrile (5 μl) to the solution, at a final concentration of 100 to 250 μM, in the presence or absence of each ligand (at a final concentration of 0–600 μM) (Ikeda, 2000). Incubation proceeded for 10 min at 37°C, and the release of RNH-6270 was measured by high-performance liquid chromatography as described above.

Chemical Modification of HSA. *Histidine Residues.* Chemical modification of His residues was performed using diethyl pyrocarbonate (Roosemont, 1978). An average of 2.22 His residues was modified out of the total of 16 His residues.

Lysine Residues. Chemical modification of Lys residues was performed according to the method of Gounaris and Perlmann (1967). The modification ratio was calculated as described by Haynes et al. (1967). An average of 3.80 of the 59 Lys residues was modified.

Tyrosine Residues. Chemical modification of Tyr residues was performed as outlined by Sokolovsky et al. (1966). An average of 1.24 of the 18 Tyr residues was modified.

Tryptophan Residues. Chemical modification of the single Trp residue was performed at room temperature (Fehske et al., 1978). An average of 0.88 of the 1 Trp residue was modified.

Chemical modifications of specific amino acid residues (Tyr, Lys, His, and Trp) were performed with the assumption that the effects on other amino acid residues would be negligible. The secondary and tertiary protein structures of all the modified HSAs were examined by circular dichroism measurements before use, and no significant difference was observed between the derivatives and native HSA (data not shown).

Synthesis and Purification of rHSA Forms. The recombinant DNA techniques used to produce wild-type rHSA and the single-residue mutants were

essentially the same as those described by Watanabe et al. (2001). A chimeric plasmid (pJDB-ADH-L10-HSA-A) containing cDNA for the mature form of HSA and an L10 leader sequence was donated by Tonen Co. (Tokyo, Japan). The mutagenic primers used (underlined letters indicate mismatches) were as follows: 5'-CAAACAGAGACTC<u>GC</u>CTGTGCCAGTCTCC-3' for K199A; 5'-GAGCTTTCAAAGCA<u>GCT</u>GCAGTAGCTCGCCTG-3' for W214A; 5'-CTATTAGTTC<u>GT</u><u>GC</u>CACCAAG-3' for Y411A.

The L10-HSA coding region was amplified by polymerase chain reaction using a forward and a reverse primer containing a 5'-terminal EcoRI site, and was cloned into the EcoRI-digested pKF19k vector (Takara Shuzo Co. Ltd.), and mutagenesis was then performed. The mutation was confirmed by DNA sequencing of the entire HSA coding region using the dideoxy chain termination method and an Applied Biosystems ABI Prism 310 Genetic Analyzer. To construct the HSA expression vector pHIL-D2-HSA, an L10-HSA coding region with or without the desired mutation site was incorporated into the methanol-inducible pHIL-D2 vector (Invitrogen). The resulting vector was introduced into the yeast species Pichia pastoris (strain GS115) to express rHSA. Secreted rHSA was isolated from the growth medium by precipitation with 60% ammonium sulfate at room temperature, and was then purified using a column of Blue Sepharose CL-6B (GE Healthcare, Little Chalfant, Buckinghamshire, UK). The eluted rHSA was deionized and then defatted using charcoal treatment.

The resulting protein exhibited a single band on an SDS/polyacrylamide gel, and all of the recombinant proteins migrated to the same position as native HSA (data not shown). Any secondary or tertiary structural differences between native (wild-type) and mutant rHSAs were analyzed by circular dichroism (data not shown). In the far-UV and near-UV regions, all rHSAs exhibited the same characteristics as native HSA.

Docking of CS-866 to HSA. To dock CS-866 to HSA, we used the crystal structure of the HSA-myristate-S-warfarin complex (PDB ID 1H9Z; Petitpas et al., 2001). The docking calculation of CS-866 to HSA was performed using SYBYL FlexX (Rarey et al., 1996). CS-866 docked at site I and site II. The residues within 5 Å from S-warfarin were defined as site I, and the residues within 5 Å from myristate-3 and -4 were defined as site II. During the docking calculation, the structure of HSA was kept rigid. The docking algorithm generated 275 and 209 different placements of CS-866 in site I and site II, respectively. All placements were evaluated using the scoring function of FlexX. For each site, because the top 10 placements exhibited nearly identical binding modes, we chose the placement with the best value as the candidate binding mode.

Refinement of Docking Models. To refine the docking models, the coordinates of CS-866 and the residues within 10 Å from CS-866 were optimized to reduce the root mean square of the gradients of potential energy to below 0.05 kcal mol⁻¹ Å⁻¹ using SYBYL 6.9.1 (Tripos, Inc., St. Louis, MO, 2003). The Tripos force field was used for the molecular energy calculation. The AMBER 7 charges (Cornell et al., 1995) were used as the atomic charges for HSA. The Gasteiger-Hückel charges (Purcel and Singer, 1967; Gasteiger and Marsili, 1980; Marsili and Gasteiger, 1980, 1981) were used as the charges for CS-866. The cut-off distance for the nonbonded interactions was 10 Å. The distance-dependent dielectric constant of 4r was used. Due to the lack of the 1st and 2nd N-terminal residues and the lack of the 585th C-terminal residue in the crystal structure of HSA, the 3rd and 584th residues were protected by an acetyl group and by an N-methyl group, respectively. The initial positions of the other missing atoms in the crystal structure were generated by SYBYL.

Statistics. Where possible, statistical analyses were performed using Student's t test

Results

Hydrolytic Kinetics. First, we were able to confirm that the hydrolysis of CS-866 by HSA followed Michaelis-Menten kinetics (data not shown). Table 1 shows the K_M, V_{max}, k_{cat}, and specificity constant (k_{cat}/K_M) values for the hydrolytic reaction.

To elucidate the reactivity of CS-866, we compared the kinetic parameters for CS-866 with those determined for the release of p-nitrophenol from PNPA (Table 2) (Means and Bender, 1975; Sakurai et al., 2004). The K_s value was found to be lower for CS-866,

TABLE 1

Kinetic parameters for the hydrolytic reaction between CS-866 and HSA at pH 7.4 and 37°C

HSA Type	K_M	V_{max}	k_{cat}	k_{cat}/K_M
	μM	$nmol \cdot min^{-1}$	min^{-1}	$\mu M^{-1} \cdot min^{-1}$
Native	48.2	1.02	0.113	0.00232

[a] Reaction conditions: 75 μM HSA, 10 to 250 μM CS-866, 1/15 M phosphate buffer (pH 7.4), 37°C.

TABLE 2

Kinetic parameters for the hydrolysis of CS-866 and PNPA by HSA at pH 7.4 and 25°C

Substrate	k_{cat}	K_s	k_{cat}/K_s
	$10^{-3} \cdot s^{-1}$	μM	$M^{-1} \cdot s^{-1}$
CS-866	0.845	42.5	19.9
PNPA	86.8	217	403.4

[a] PNPA data from Sakurai et al. (2004).

TABLE 3

Thermodynamic parameters for the hydrolysis of CS-866 and PNPA by HSA

Substrate	ΔG_I	ΔG_s	ΔG	ΔH	ΔS
	$kJ \cdot mol^{-1}$	$kJ \cdot mol^{-1}$	$kJ \cdot mol^{-1}$	$kJ \cdot mol^{-1}$	$kJ \cdot mol^{-1} \cdot K^{-1}$
CS-866	71.3	-25.0	96.3	34.7	-0.207
PNPA[a]	58.1	-20.9	79.0	66.1	-0.0435

[a] PNPA data from Sakurai et al. (2004). Reaction conditions: 1/15 M phosphate buffer (pH 7.4), 25°C.

suggesting that PNPA has greater affinity than CS-866 for HSA (Fersht, 1998; Sakurai et al., 2004). The catalytic rate constant, k_{cat}, was also found to be greater for PNPA.

Thermodynamics. The relationship between the catalytic rate constants and temperature followed the Arrhenius equation. Accordingly, a linear relationship was found between ln k_{cat} and $1/T$, where T is the absolute temperature in degrees Kelvin (data not shown). The activation energy of the reaction, E_a, calculated from the Arrhenius plot (Fersht, 1998; Sakurai et al., 2004), was found to be 37.1 kJ · mol⁻¹.

Using the HSA-hydrolysis parameters, we compared energy changes and thermodynamic parameters between CS-866 and PNPA (Table 3). CS-866 had larger values of ΔG (96.3 kJ · mol⁻¹) and ΔS (-0.207 kJ · mol⁻¹ · K⁻¹) than PNPA.

Effects of Ligands on Hydrolysis. The site I-specific ligands warfarin, DNSA, and n-butyl p-AB were used as inhibitors to investigate for any competition with the hydrolytic reaction (Yamasaki et al., 1996; Kragh-Hansen et al., 2002). Interestingly, warfarin inhibited hydrolysis in a competitive manner, with a K_i value of 155 μM in a Dixon plot (Fig. 2A). By contrast, neither n-butyl p-AB nor DNSA inhibited HSA-catalyzed hydrolysis of CS-866 (Fig. 2, B and C).

The site II-specific ligands ibuprofen and diazepam were used to investigate, whether there is competition between that ligand-binding site and the catalytic site (Kragh-Hansen et al., 2002). Diazepam had no inhibitory effect, but competitive inhibition was observed with ibuprofen, with a K_i value of 235 μM in a Dixon plot (Fig. 3A and 3B).

Effect of Chemical Modification on Hydrolysis. Hydrolytic activities of the four specifically modified HSA derivatives (Tyr-, Lys-, His-, and Trp-HSA) were assayed (Fig. 4). Compared with native-type HSA, all modified HSA derivatives had significantly decreased hydrolytic activity ($p < 0.05$). Modification of Lys residues or of the single Trp residue resulted in the most pronounced reductions in catalytic reactivity.
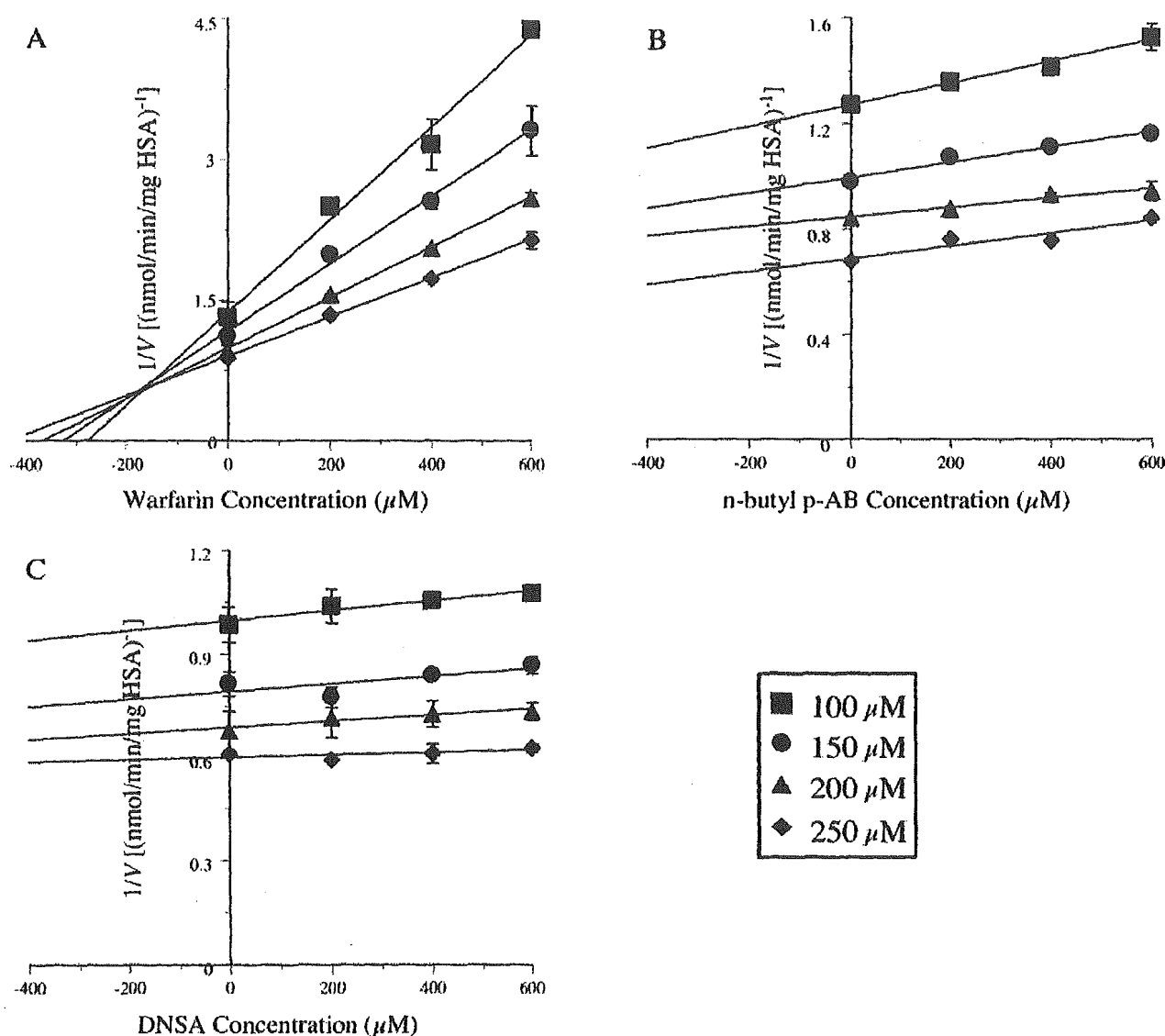
Legend:
- ■ 100 μM
- ● 150 μM
- ▲ 200 μM
- ◆ 250 μM

Fig. 2. Effect of warfarin (A), n-butyl p-AB (B), and DNSA (C) (0–600 μM) on the hydrolysis of CS-866 by HSA. Reaction conditions: 75 μM HSA, 100 to 250 μM CS-866. 1/15 M phosphate buffer (pH 7.4). 37°C. Plots represent mean ± S.D. (n = 3).

Examination of Hydrolytic Activity Using Site-Directed Mutagenesis. Wild-type rHSA and the HSA single-residue mutants K199A, W214A, and Y411A were used to examine involvement of various amino acid residues in the hydrolysis. The hydrolytic activity of each rHSA was examined to elucidate the contribution of specific amino acid residues (Fig. 5). Compared with the wild-type rHSA, all mutant rHSAs showed significant decreases in catalytic activity. K199A exhibited a particularly marked decrease in catalytic activity (p < 0.01), suggesting that Lys-199 plays a particularly important role in the hydrolysis. These results are in good agreement with those obtained with the chemically modified HSAs. The W214A and Y411A mutants showed a significant reduction in catalytic activity (p < 0.05), indicating that the amino acid residues Trp-214 and Tyr-411 are also involved in the hydrolytic reaction.

Molecular Interaction of CS-866 and HSA in Docking Models. We obtained two docking models: model I for site I, and model II for site II. In model I, the binding of CS-866 was similar to that of

warfarin (Fig. 6). The biphenyl moiety of CS-866 was bound to the hydrophobic pocket consisting of Leu-219, Leu-238, Val-241, Leu-260, Ala-261, Ile-264, Ile-290, and Ala-291. The 2-propyl-imidazole moiety and the propan-2-ol moiety were bound to the other hydrophobic pocket (Phe-211, Trp-214, Ala-215, Leu-219, and Leu-238). Hydrogen bonds to and electrostatic interactions with other residues are detailed in Table 4. Oxygen atoms of the vinylene carbonate moiety formed hydrogen bonds with side chains of Arg-218 and of Arg-222. Negative charges of the tetrazole moiety interacted electrostatically with side chains of Lys-199 and of Arg-257. The hydroxyl oxygen atom of the propan-2-ol moiety formed a hydrogen bond with the side chain of Lys-199, and the hydrogen atom formed a hydrogen bond with the side chain of His-242. The carbonyl oxygen atom of the ester moiety formed a hydrogen bond with the side chain of Lys-199. The ester moiety of CS-866 was in the vicinity of Glu-292. However, the side chain of Glu-292 was distant from the carbonyl carbon of the ester moiety, because the docking program, FlexX, cannot account for chemical reactions and remains rigid. We changed the torsion angles
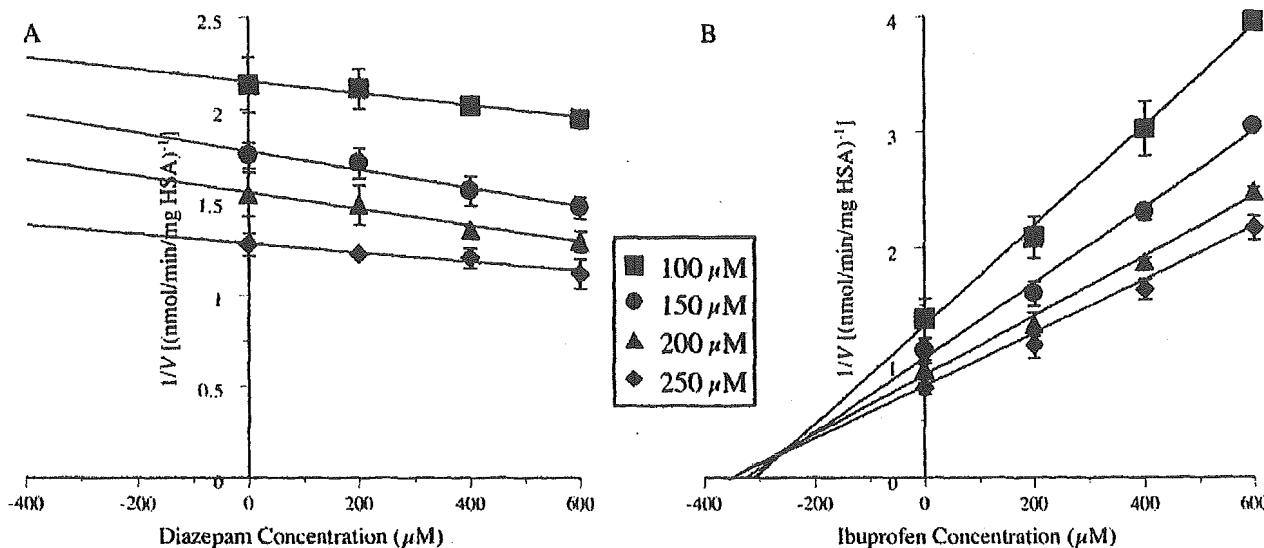
Fig. 3. Effect of diazepam (A) and ibuprofen (B) (0~600 μM) on the hydrolysis of CS-866 by HSA. Reaction conditions: 75 μM HSA, 100 to 250 μM CS-866, 1/15 M phosphate buffer (pH 7.4), 37°C. Plots represent mean $\pm$ S.D. ($n = 3$).
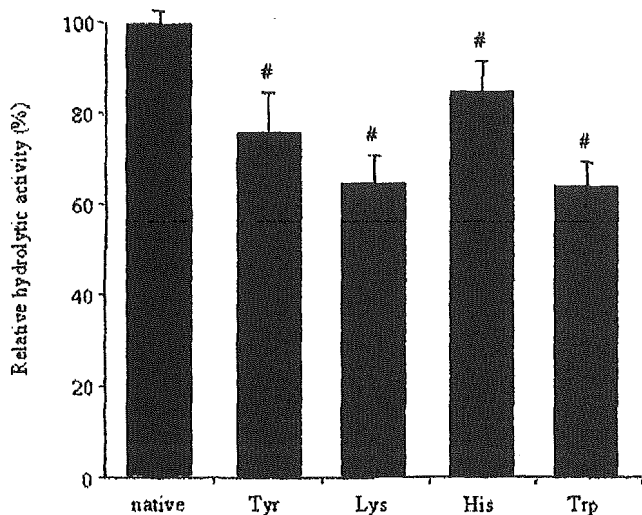

Fig. 4. Hydrolytic activities of chemically modified HSAs as compared with that of normal HSA. Reaction conditions: 75 μM HSA, 250 μM CS-866, 1/15 M phosphate buffer (pH 7.4), 37°C. Each column represents mean $\pm$ S.D. ($n = 3$). #, significantly different from native-type HSA ($p < 0.05$).
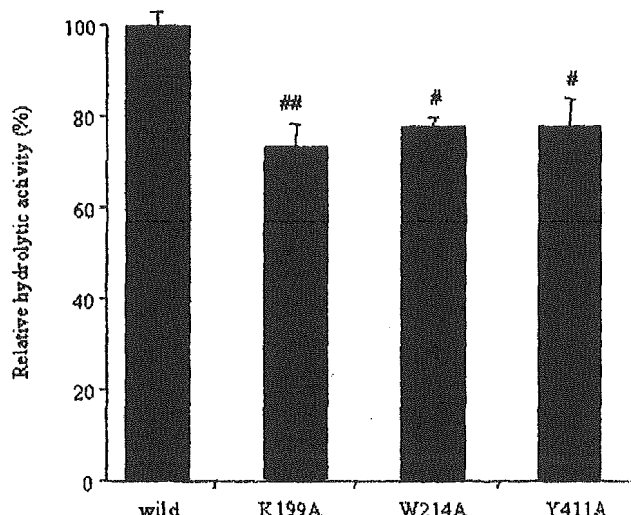

Fig. 5. Hydrolytic activities of mutant rHSAs as compared with that of wild-type rHSA. Reaction conditions: 75 μM HSA, 250 μM CS-866, 1/15 M phosphate buffer (pH 7.4), 37°C. Each column represents mean $\pm$ S.D. ($n = 3$). #, $p < 0.05$, and ##, $p < 0.01$ as compared with wild-type rHSA.

of the side chain of Glu-292 without steric hindrance as Glu-292 became capable of a nucleophilic reaction.

In model II, CS-866 was bound to site II using the pocket for myristate-4 (Fig. 7) (Curry et al., 1998). The pocket for myristate-3 was not occupied. The biphenyl moiety and the 2-propyl-imidazole moiety were bound to the hydrophobic pocket consisting of Leu-387, Pro-486 and Ala-490. The propan-2-ol moiety was surrounded by the hydrophobic residues (Leu-387, Leu-430, and Leu-453). Table 5 shows hydrogen bonds and electrostatic interactions in site II. Negative charges of the tetrazole moiety interacted electrostatically with the side chain of Arg-485, and the tetrazole moiety formed a hydrogen bond with the side chain of Asn-391. The side chain of Ser-489 formed hydrogen bonds with the hydroxyl oxygen atom of the propan-2-ol moiety and the carboxyl oxygen atom of the ester moiety. The carbonyl oxygen atom of the ester moiety

formed a hydrogen bond with the side chain of Lys-414. The carboxyl oxygen atom of the ester moiety formed a hydrogen bond with the side chain of Tyr-411.

Discussion

This antihypertensive prodrug, CS-866, is hydrolyzed in the serum. Hydrolysis of CS-866 in serum has been observed in several species, and comparison among five species has shown that hydrolytic activity is highest in rabbits, followed by dogs, mice, rats, and humans (Ikeda, 2000). Furthermore, we examined the activity due to serum albumin. It was found to be highest in humans, followed by rats, mice, rabbits, and dogs (data not shown). This indicates that the mechanisms of hydrolysis of CS-866 in serum differ among those species, and that HSA plays a more important role in producing RNH-6270 than other serum albumin species.
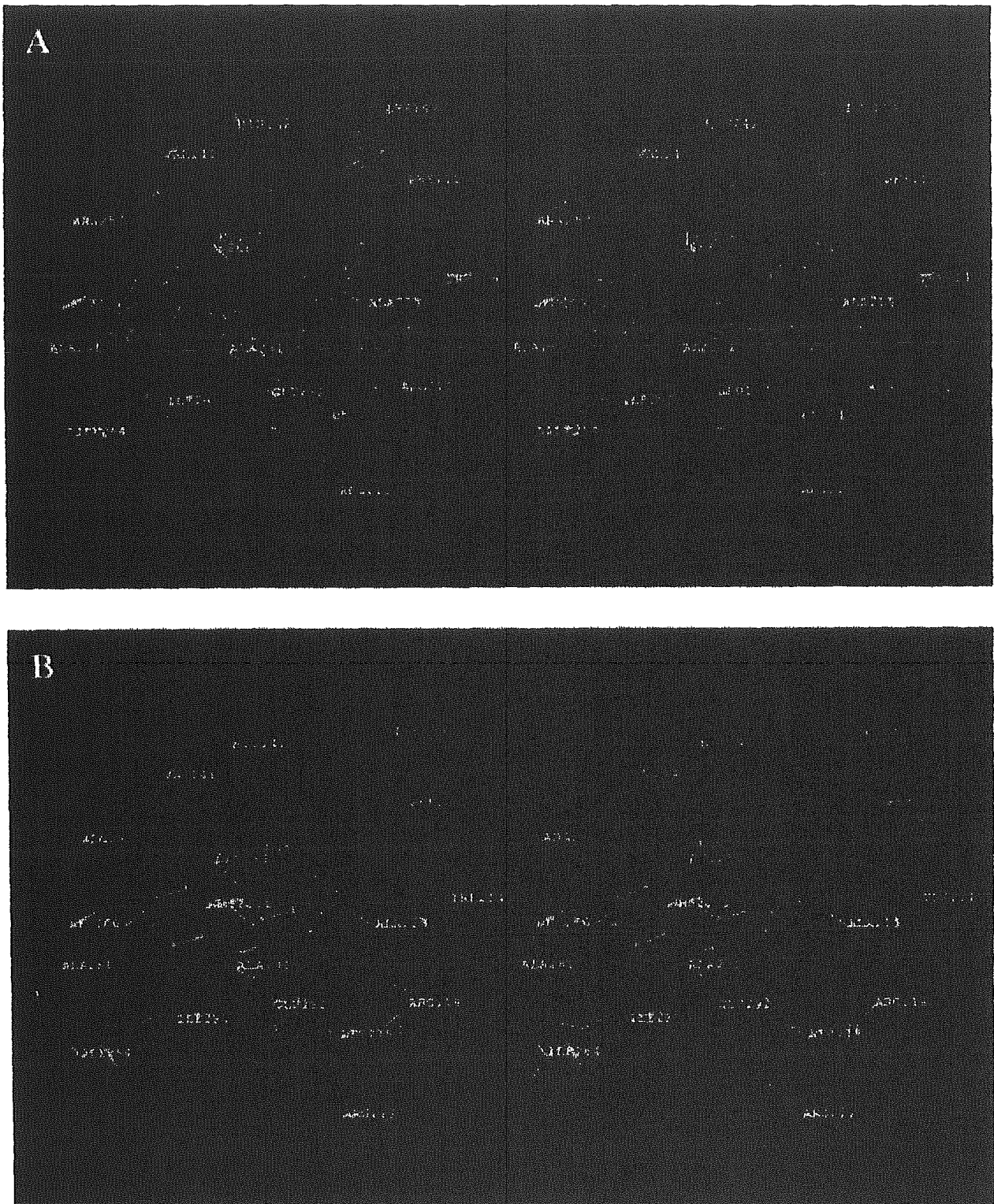
Fig. 6. Stereo drawings of ligands in site I. A, modeling structure for CS-866. The torsion angles of the side chain of Glu-292 were changed as Glu-292 becomes capable of a nucleophilic reaction. B, crystal structure for S-warfarin (PDB ID 1H9Z). Relaxed stereo viewing.

TABLE 4

Hydrogen bonds and electrostatic interactions in model I of HSA-CS-866 complex

Donor		Acceptor		Distance
				Å
Hydrogen bonds				
Lys-199	N_ζ	Ester	C=O	4.1
	N_ζ	Propan-2-ol	OH	3.0
Propan-2-ol	OH	His-242	Nε2	4.6
Arg-218	N_ϵ	Vinylene carbonate	O2	3.8
	$N_{\eta}2$		C=O	3.4
Arg-222	$N_{\eta}2$		Cl	3.1
Positive		Negative		
Electrostatic interactions				
Lys-199	N_ζ	Tetrazole	N2	5.7
Arg-257	N_ϵ		N4	2.8

Thermodynamic Properties. The esterase-like activity of HSA is dependent on the catalytic rate constant, k_{cat}, and increases with a decrease in the activation free energy change, ΔG. Thus, the magnitude of ΔG, which is dependent on activation entropy change (ΔS), as calculated from a thermodynamic analysis, can be regarded as an indicator of hydrolytic activity of HSA (Fersht, 1998; Sakurai et al., 2004). Because PNPA has lower ΔG and ΔS values than CS-866 (Table 3), PNPA exhibited greater affinity for HSA and a higher catalytic rate than CS-866 (Table 2). Hydrolysis reactions catalyzed by albumin have previously been found to have a particularly great entropy difference between the ground state (ES) and the transition state (ES*) (Sakurai et al., 2004). The active sites of HSA to which the substrate binds are perfectly oriented to the reactive site of the substrate (the ester portion) for hydrolysis, and thus has a smaller entropy difference between the transition state (ES*) and the ground state (ES). This may be the reason why hydrolysis of PNPA proceeds more readily than hydrolysis of CS-866. That is, compared to CS-866, PNPA has a structure and orientation that are better suited to hydrolysis by HSA.

Relationship Between Ligand Binding Sites and Hydrolytic Active Sites. HSA is the most abundant protein in blood plasma and serves as a storage protein and transport protein for many endogenous and exogenous compounds (Peters, 1996; Kragh-Hansen et al., 2002). The unique capability of HSA to reversibly bind a large number of compounds is usually explained by the existence of a number of binding regions (including site I and site II), each of which has a very different specificity (Kragh-Hansen, 1991; Kragh-Hansen et al., 2002). Furthermore, site I on HSA consists of three subsites: Ia, Ib, and Ic (Fehske et al., 1982; Yamasaki et al., 1996). Another important role of HSA is as a catalyst for the hydrolysis of various compounds, such as esters, amides, and phosphates. It has been suggested that the active site of HSA for *p*-nitrophenyl esters is site II, and that Tyr-411 is essential for hydrolysis of *p*-nitrophenyl esters (Ozeki et al., 1980; Watanabe et al., 2000). The reactive site and active residue for nitroaspirin are reportedly site I and Lys-199, respectively (Ikeda and Kurono, 1986). The relationship between the hydrolytic active sites of HSA for CS-866 and the proteins' ligand-binding sites was investigated in the present study.

There are interesting patterns of competition between site I and site II ligands for hydrolysis. Although warfarin, which is regarded as a typical ligand of subsite Ia of HSA, acts as a competitive inhibitor, this does not necessarily indicate that the HSA catalytic site for CS-866 is subsite Ia, because ibuprofen, a typical site II ligand, also exhibited evidence of competitive inhibition (Figs. 2A and 3B). These results suggest that substrate specificity of the esterase-like region and

ligand-binding site of HSA is inconsistent. In other words, the catalytic site for CS-866 on HSA may recognize CS-866 in a manner different from that of the ligand-binding site.

Roles of Specific Amino Acid Residues. For proteins whose X-ray crystallographic structure is known, the role of each amino acid residue can be quantitatively determined using the amino acid displacement (site-directed mutagenesis) technique and information obtained from X-ray analysis.

The present chemical modification experiments indicate that Lys, Trp, and Tyr residues of HSA are important for hydrolysis of CS-866 by HSA, and that His residues are also involved (Fig. 4). These experiments were performed with mildly modified HSA, because, for example, only 1.24 of the Tyr residues and 3.8 of the Lys residues were modified. However, HSA has 59 Lys residues, and the numbers of Trp, Tyr, and His residues are 1, 18, and 16, respectively. Previous findings have demonstrated that Tyr-411 is most likely the reactive Tyr of HSA (Watanabe et al., 2000). It is also known that the reactivity of Lys-199 is high (Means and Bender, 1975). Furthermore, it is reported that this single Trp residue contributes to the esterase-like activity of HSA (Ozeki et al., 1980; Kurono et al., 1982). In an attempt to identify specific residues of importance for the hydrolysis of CS-866, we examined the activity of several rHSAs, namely wild-type HSA and the single-residue mutants K199A, W214A, and Y411A.

Because we did not observe a great decrease of the hydrolytic activity of HSA for CS-866, even in the single-residue mutants K199A and Y411A, we conclude that the catalytic sites of HSA for CS-866 are not solely confined to the Lys-199 and Tyr-411 residues but, rather, involves several additional amino acid residues (Fig. 5).

The single Trp residue, Trp-214, is located close to Lys-199, as indicated by X-ray diffraction analysis, and is an element of a major interdomain cluster of hydrophobic residues (He and Carter, 1992; Sugio et al., 1999). The mutant W214A exhibited a significant decrease in hydrolytic activity (Fig. 5). In addition, the microenvironment near Trp-214 was investigated to obtain detailed information about the role of this residue in the hydrolysis. After incubation with CS-866 for 10 min, the relative fluorescence intensity of HSA decreased by more than half and the λ_{max} was blue-shifted (data not shown). These results are consistent with a model indicating that the Trp-214 residue is involved in hydrolytic reaction. These limited data lead us to the idea that a double (or triple) mutation of Lys-199, Trp-214, and Tyr-411 could completely abolish the hydrolytic activity. Further investigations on this point are under way at this laboratory.

Structural Mechanism of Hydrolysis Based on Models. The present findings suggest that HSA has two catalytic sites for CS-866, for the following two reasons. Mutation at site I or site II diminishes but does not abolish the hydrolytic activity. The hydrolytic activity is inhibited by both warfarin (site I drug) and ibuprofen (site II drug).

In model I (Fig. 6), CS-866 occupied the binding site of warfarin; this is consistent with the results showing that warfarin inhibits the hydrolytic activity of HSA. In site I, the carbonyl oxygen atom of the ester moiety formed a hydrogen bond with the side chain of Lys-199, and this hydrogen bond could function as an oxyanion hole. The importance of Lys-199 indicated by the model is consistent with the decreased hydrolytic activity of the K199A mutant and the HSA variant produced by chemical modification of Lys. The catalytic residue may be Glu-292; the distance between the oxygen atom of the side chain of Glu-292 and the carbonyl carbon of the ester moiety of CS-866 was 4.8 Å. The hydrophobic interaction between CS-866 and Trp-214 indicated by the model is consistent with the diminished
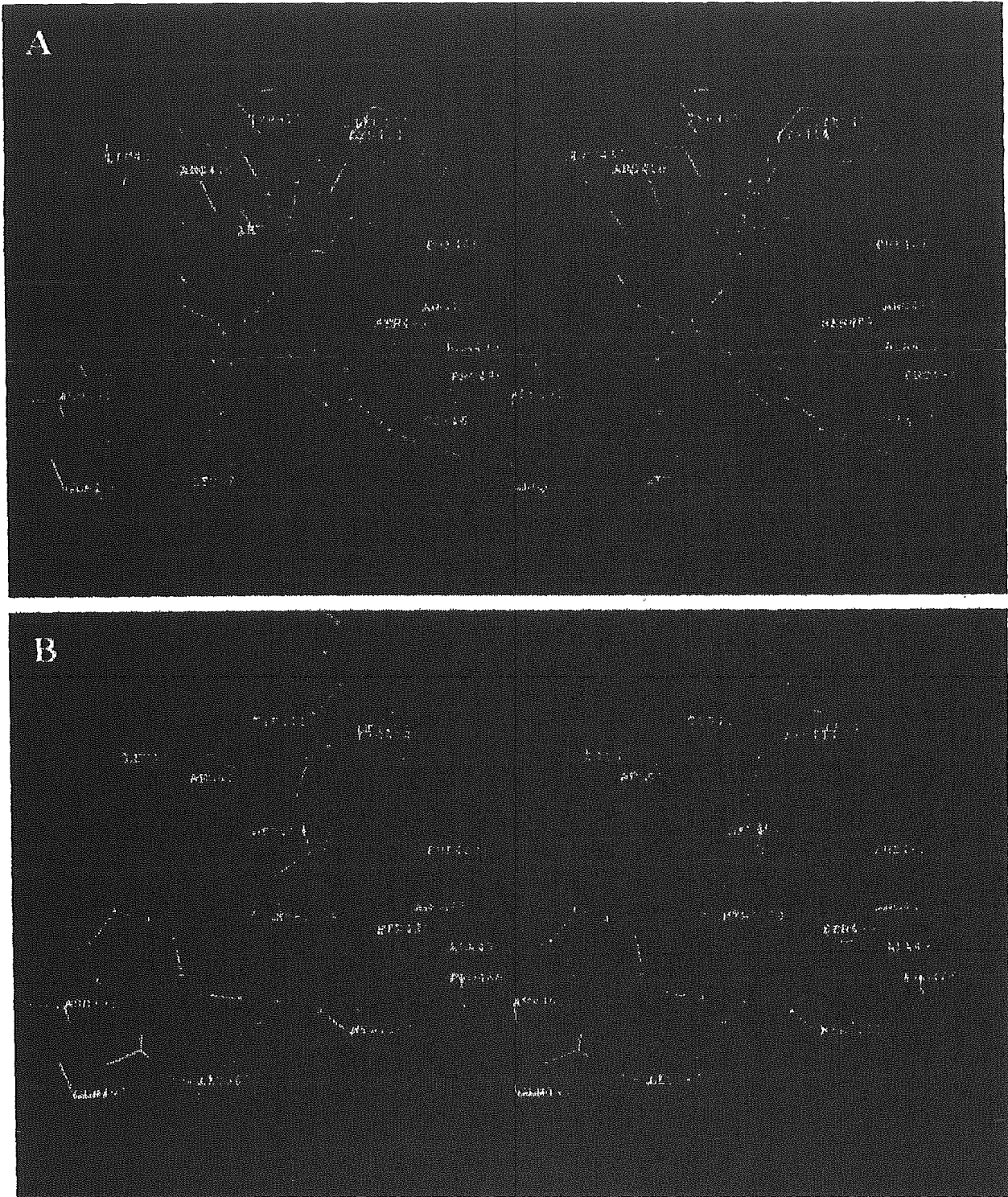
Fig. 7. Stereo drawings of ligands in site II. A, modeling structure for CS-866; B, crystal structure for myristate-3 and -4 (PDB ID 1H9Z). Relaxed stereo viewing.

hydrolytic activity of the W214A mutant and the HSA variant produced by chemical modification of Trp.

Model II (Fig. 7) indicates that the mechanism of hydrolysis of CS-866 is almost the same as that found in previous studies for p-nitrophenyl esters, with the exception of the involvement of Arg-410 (Watanabe et al., 2000; Sakurai et al., 2004). Instead of Arg-410, Lys-414 was used to create an oxyanion hole. The distance between the hydroxyl oxygen atom of Tyr-411 and the carbonyl carbon of the

TABLE 5

Hydrogen bonds and electrostatic interactions in model II of HSA-CS-866 complex

Donor		Acceptor		Distance
				Å
Hydrogen bonds				
Asn-391	N_x2	Tetrazole	N2	2.9
Tyr-411	O_η	Ester	-O-	2.8
Lys-414	N_ζ		C=O	2.7
Ser-489	O_γ		-O-	4.7
	O_γ	Propan-2-ol	OH	4.1
Positive		Negative		
Electrostatic interactions				
Arg-485	$N_\eta1$	Tetrazole	N3	3.5

ester moiety of CS-866 was 3.3 Å, indicating that it is possible that Tyr-411 plays the role of a cathartic residue. The importance of Tyr-411 and Lys-414 is consistent with the decreased hydrolytic activity of the Y411A mutant and of the HSA variants produced by chemical modification of Tyr or Lys. In our model II, CS-866 was bound to the pocket for myristate-4 in site II. The binding pockets of the site II ligands ibuprofen and diazepam are unknown. If ibuprofen binds to the pocket for myristate-4, our model II provides a mechanism for inhibition of hydrolytic activity of HSA by ibuprofen.

The present findings indicate that hydrolysis of CS-866 by HSA is dependent on ΔS. Another important factor is the orientation between the catalytic active site on HSA and the ester region of the substrate. There are differences between the catalytic active sites and the ligand-binding sites of HSA. Furthermore, the residues of Lys-199, Trp-214, and Tyr-411 play important roles in this catalytic reaction. All of these experimental findings are consistent with the docking model that we derived from computer simulation.

References

Brousil JA and Burke JM (2003) Olmesartan medoxomil: an angiotensin II-receptor blocker. *Clin Ther* 25:1041–1055.

Chen RF (1967) Removal of fatty acids from serum albumin by charcoal treatment. *J Biol Chem* 242:173–181.

Curry S, Mandelkow H, Brick P, and Franks N (1998) Crystal structure of human serum albumin complexed with fatty acid reveals an asymmetric distribution of binding sites. *Nat Struct Biol* 5:827–835.

Cornell WD, Cieplak P, Bayly CI, Gould IR, Merz KM Jr, Ferguson DM, Spellmeyer DC, Fox T, Caldwell JW, and Kollman PA (1995) A second generation force field for the simulation of proteins, nucleic acids and organic molecules. *J Am Chem Soc* 117:5179–5197.

Fehske KJ, Müller WE, and Wollert U (1978) The modification of the lone tryptophan residue in human serum albumin by 2-hydroxy-5-nitrobenzyl bromide. Characterization of the modified protein and the binding of L-tryptophan and benzodiazepines to the tryptophan-modified albumin. *Hoppe-Seylers Z Physiol Chem* 359:709–717.

Fehske KJ, Schläfer U, Wollert U, and Müller WE (1982) Characterization of an important drug binding area on human serum albumin including the high-affinity binding sites of warfarin and azapropazone. *Mol Pharmacol* 21:387–393.

Fersht A (1999) *Structure and Mechanism in Protein Science*, Freeman, New York.

Gasteiger J and Marsili M (1980) Iterative partial equalization of orbital electronegativity: a rapid access to atomic charges. *Tetrahedron* 36:3219–3228.

Gasteiger J and Marsili M (1981) Prediction of proton magnetic resonance shifts: the dependence on hydrogen charges obtained by iterative partial equalization of orbital electronegativity. *Organ Magn Reson* 15:353–360.

Gounaris AD and Perlmann GE (1967) Succinylation of pepsinogen. *J Biol Chem* 242:2739–2745.

Haynes R, Osuga DT, and Feeney RE (1967) Modification of amino groups in inhibitors of proteolytic enzymes. *Biochemistry* 6:541–547.

He XM and Carter DC (1992) Atomic structure and chemistry of human serum albumin. *Nature (Lond)* 358:209–215.

Ikeda K and Kurono Y (1986) Enzymatic activity and drug binding activity of human serum albumin. *Yakugaku Zasshi* 106:841–855.

Ikeda T (2000) Two prodrugs activated by serum esterases including albumin. Proceedings of the International Symposium on Serum Albumin & α_1-Acid Glycoprotein 173–180.

Koike H, Sada T, and Mizuno M (2001) In vitro and in vivo pharmacology of olmesartan medoxomil, an angiotensin II type AT1 receptor antagonist. *J Hypertens Suppl* 19:1:S3–S14.

Kragh-Hansen U (1991) Octanoate binding to the indole- and benzodiazepine-binding region of human serum albumin. *Biochem J* 273:641–644.

Kragh-Hansen U, Chuang VTG, and Otagiri M (2002) Practical aspects of the ligand-binding and enzymatic properties of human serum albumin. *Biol Pharm Bull* 25:695–704.

Kurono Y, Yamada H, and Ikeda K (1982) Effects of drug binding on the esterase-like activity of human serum albumin. V. Reactive site towards substituted aspirins. *Chem Pharm Bull* 30:296–301.

Marsili M and Gasteiger J (1980) Pi-Charge Distributions from Molecular Topology and Pi-Orbital Electronegativity. *Croat Chem Acta* 53:601–614.

Means GE and Bender ML (1975) Acetylation of human serum albumin by p-nitrophenyl acetate. *Biochemistry* 14:4989–4994.

Neutel JM (2001) Clinical Studies of CS-866, the newest angiotensin II receptor antagonist. *Am J Cardiol* 87 (8A):37C–43C.

Ozeki Y, Kurono Y, Yotsuyanagi T, and Ikeda K (1980) Effects of drug binding on the esterase activity of human serum albumin: inhibition modes and binding sites of anionic drugs. *Chem Pharm Bull* 28:535–540.

Peters T Jr (1996) *All about Albumin. Biochemistry, Genetics and Medical Applications*. Academic Press, San Diego.

Petitpas I, Bhattacharya AA, Twine S, East M, and Curry S (2001) Crystal structure analysis warfarin binding to human serum albumin: anatomy of drug site I. *J Biol Chem* 276:22804–22809.

Purcel WP and Singer JA (1967) A brief review and table of semiempirical parameters used in the Hückel molecular orbital method. *J Chem Eng Data* 12:235–246.

Rarey M, Kramer B, Lengauer T, and Klebe G (1996) A fast flexible docking method using incremental construction algorithm. *J Mol Biol* 261:470–489.

Roosemont JL (1978) Reaction of histidine residues in proteins with diethylpyrocarbonate: differential molar absorptivities and reactivities. *Anal Biochem* 88:314–320.

Sakurai Y, Ma SF, Watanabe H, Yamaotsu N, Hirono S, Kurono Y, Kragh-Hansen U, and Otagiri M (2004) Esterase-like activity of serum albumin: characterization of its structural chemistry using p-nitrophenyl esters as substrates. *Pharm Res (NY)* 21:285–292.

Sokolovsky M, Riordan JF, and Vallee BL (1966) Tetranitromethane. A reagent for the nitration of tyrosyl residues in proteins. *Biochemistry* 5:3582–3589.

Sugio S, Kashima A, Mochizuki S, Noda M, and Kobayashi K (1999) Crystal structure of human serum albumin at 2.5 Å resolution. *Protein Eng* 12:439–446.

Watanabe H, Tanase S, Nakajou K, Maruyama T, Kragh-Hansen U, and Otagiri M (2000) Role of Arg-410 and Tyr-411 in human serum albumin for ligand binding and esterase-like activity. *Biochem J* 349:813–819.

Watanabe H, Yamasaki K, Kragh-Hansen U, Tanase S, Harada K, Suenaga A, and Otagiri M (2001) In vitro and in vivo properties of recombinant human serum albumin from Pichia pastoris purified by a method of short processing time. *Pharm Res (NY)* 18:1775–1781.

Yamasaki K, Maruyama T, Kragh-Hansen U, and Otagiri M (1996) Characterization of site I on human serum albumin: concept about the structure of a drug binding site. *Biochim Biophys Acta* 1295:147–157.

Address correspondence to: Professor Masaki Otagiri, Ph D, Department of Biopharmaceutics, Graduate School of Pharmaceutical Sciences, Kumamoto University, 5-1 Oe-honmachi, Kumamoto 862-0973, Japan. E-mail. otagirim@gpo.kumamoto-u.ac.jp